

Development and simulation of an active target detector with GEM foil readout

Thesis to reach a degree of Master of Science

by

Elisabeth Rickert

09.05.2017



LUND UNIVERSITY



JOHANNES GUTENBERG
UNIVERSITÄT MAINZ

Nuclear Physics Department

Supervisors Lund University:
Joakim Cederkäll, Pavel Golubev

Supervisor JGU Mainz:
Klaus Wendt

Abstract

At CERN, radioactive ion beams with energies of up to 10 MeV/u can be produced by a newly commissioned post-accelerator, HIE-ISOLDE, which expands the possibilities for nuclear reaction studies. To investigate the collision properties of the ion beam with a target, an active gas–target detector is under development by the Reactions Group at the Nuclear Physics Division in Lund. The existing detector setup was further investigated in this thesis. Experimental tests of the gain and stability of the detector were performed with the simulation package Garfield++ for a 82/18 Ar/CO₂ gas mixture and a ⁵⁵Fe source. The results were compared to results obtained from an earlier project. Simulations of electron drift were performed for different drift distances to characterize the spread of an electron cloud to design a new backgammon shaped readout plane to investigate the electron diffusion. First tests of new readout electronics have been performed and a C++ file has been written to investigate cross talk of the used Kapton cables.

Contents

1	Introduction	1
2	Active Target Gas Detector	4
2.1	Interaction of photons and charged particles with matter	4
2.2	Drift and diffusion	5
2.3	Avalanche multiplication	6
2.4	Penning and quenching effects	6
2.5	Proportional counter	7
2.6	Gas Electron Multiplier	8
2.6.1	Operational principle	8
2.6.2	Gain	10
2.7	Time Projection Chamber	11
2.8	Readout	12
3	Measurements with GEM foils	15
3.1	Assembly	15
3.2	Setup	18
3.3	Rate and gain	19
3.3.1	Voltage divider	19
3.3.2	Direct voltage supply	24
4	Simulation	28
4.1	Simulation Procedure	28
4.1.1	gmsht	28
4.1.2	Elmer	29
4.1.3	Garfield++	30
4.2	Number of primaries, gain and signal	31
4.3	Electron spread	32
5	Data readout and Crosstalk	36
6	Results and Conclusion	44
7	Outlook	46

Contents

8	Appendix	47
8.1	Drift and velocity simulation	47
8.2	C-file	52

1 Introduction

This project concerns the development of an active gas-target detector for experiments with radioactive ion beams. The detector can be used for two different purposes. On the one hand, products from reactions can be tracked in the gas volume to reconstruct reaction kinematics. On the other hand, the detector can also be used to determine the components of the radioactive ion beam itself. A detector of this kind has applications in both pure nuclear physics and nuclear astrophysics.

Nuclear astrophysics, investigating the creation of the elements, is a topic of long standing interest, which today is examined in connection with the processes that occur during different stages of stellar evolution. Radioactive ion beams give new opportunities in this field, since they make it possible to study nuclear reactions with unstable atomic nuclei that occur in stars. Radioactive ion beams are e.g. needed to understand the rapid neutron capture process (r-process), that is believed to occur in supernova explosions, where heavy elements above iron are produced. When it comes to the abundance of proton rich nuclei, the rapid proton capture process (rp-process) plays a similar role [1]. The rp-process occurs after the CNO cycle in novae or X-ray bursters for high pressures and temperatures. The reaction path of the thermonuclear runaway approaches the proton drip line in an analogue way to how the r-process path approaches the neutron drip line. Elements from neon to iron and even further can be produced in this process, whereby the power generation can exceed the CNO cycle by a factor of ~ 100 [1].

At ISOLDE, radioactive beams are generated by letting a proton beam at ~ 1 GeV hit a thick target, typically of a high-Z element, to produce unstable isotopes by fragmentation, spallation and fission. The beam is ionized, often via resonant laser ionization, before being extracted over a 60 keV potential difference. After extraction, the beam is mass separated, cooled and finally post-accelerated to a secondary target station where the experiments take place. In the newly commissioned post-accelerator, HIE-ISOLDE, ion beam energies of up to 10 MeV/u will be reached giving rise to new possibilities for nuclear reaction studies. An overview of the ISOLDE facility is shown in Figure 1.1.

In nuclear astrophysics as well as in pure nuclear physics it is often interesting to study resonant states in unstable nuclei, which can be done by scattering a radioactive beam on a solid target. When one wants to examine proton pick-up

1 Introduction

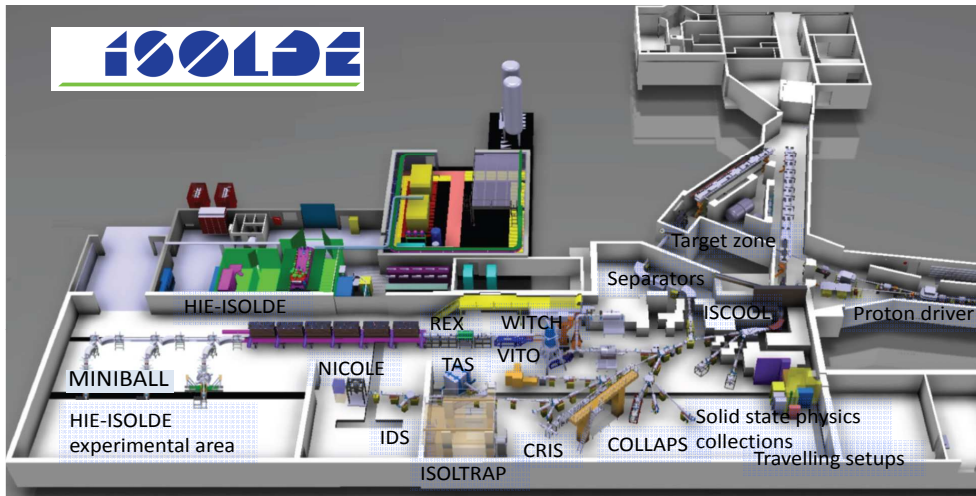


Figure 1.1: Overview of the ISOLDE facility. The beam is shot in from the right hand side, where also the target station is placed. HIE-ISOLDE is shown on the left hand side of the picture.

reactions or proton resonances such targets are typically made of thin plastic foils of polyethylene (PE). To cover the energy range of a certain resonance one can either vary the beam energy from the accelerator in small steps, or use a thick target and let the incoming beam lose energy by stopping. In that case, reactions will consequently occur at different depths and therefore at varying interaction energies. This approach takes less time than to vary the beam energy to cover the region of interest in the energy spectrum. Nevertheless, the energy resolution is affected by this approach and the interaction energies must be calculated e.g. from the stopping power in the target or be deduced from simulations.

In traditional scattering experiments, light projectile beams are shot onto a heavier target in what is called normal kinematics. When a heavy beam is instead shot at a light target, e.g. a gas or solid containing hydrogen or helium, the reaction is said to be performed in inverse kinematics. Inverse kinematics experiments offer special advantages and are frequently of interest in radioactive beam experiments. The reason is that beams of radioactive i.e., beta-unstable, ions can be used in reactions even if they are too short-lived to be used as target material. Since the incoming particle can be stopped in the target, all resonant energies can be observed in one run. The scattered particles, e.g. protons that have a lower Z than the beam and can exit the target, are detected in forward angles. For a solid target this method has the disadvantage that different interaction energies, from reactions that occurred at different distances along the beam path in the target, can correspond to the same scattering angle in the detector. Consequently, the resolution is affected.

In order to improve on this problem, an active target detector can be used. One

1 Introduction

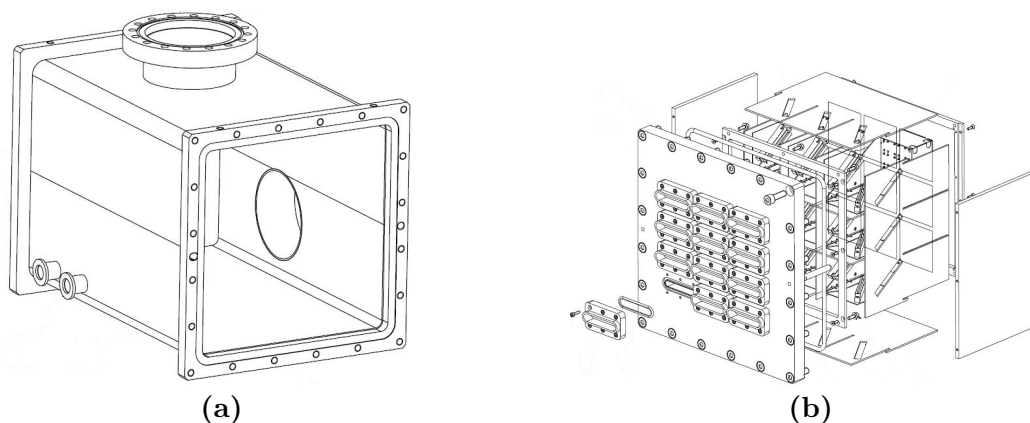


Figure 1.2: Panel (a): 3D-model of the final scattering chamber, without readout plane. Panel (b): The charged particle detector mounting.

such example is a gaseous ionization detector, in which the gas atoms are used as a target. If the detector works as a time projection chamber (TPC), both the incoming beam and the reaction products are tracked, so that the reaction vertex can be reconstructed. Therefore, the angles of the outgoing particles can be determined precisely and a large target can be used without suffering resolution deterioration. From the length of the track and the amplitude of the produced signals, the energy of the reaction products can also be determined. Moreover, the detected particles can be identified by their specific energy loss in the gas. By varying the pressure of the gas, several target thicknesses can be imitated, so that under the right conditions heavy particles can be stopped while lighter ones travel on after the recoil. In this case, sensitive detectors can be used to detect and track light reaction products in forward angles without being destroyed by the beam.

To investigate the processes discussed above, an active target gas detector is under development by the Reactions Group at the Nuclear Physics Division in Lund. Gas Electron Multiplier (GEM) foils, used to amplify the electrons before the readout, are used to track the particles in the gas volume of the detector. The first steps to examine and characterize the GEM foil behaviour have been performed in an earlier MSc project [2]. The existing setup is further investigated in this thesis, including extended experimental tests of the gain and stability of the detector, simulations of electron drift in a large drift volume, and first tests of new read-out electronics. The performance of the new electronics is characterized concerning cross-talk, and the drift range for the incoming particles is examined. For the latter purpose, simulations with Garfield++ are carried out to predict the detector response for different gas pressures. Of special interest here was to simulate the spread of the electron cloud to give information to the design for the readout planes to be used. For safety reasons the laboratory measurements were done at one atmosphere pressure.

2 Active Target Gas Detector

To detect incoming radiation, to track position and to measure energy of the interacting particles, a detector has to fulfil several requirements. As discussed in the introduction, an active gas-target detector is used for this purpose. The incoming particle can ionize the gas and the electrons produced in this process can be collected on an anode plane and a signal be read out. The measured signal is the evidence of an interaction between the incoming radiation and the detector gas. In the following section, the basic principles and the possible interactions that can occur are described, and different readout principles are presented.

2.1 Interaction of photons and charged particles with matter

If interactions of radiation and matter are examined, two different cases must be distinguished, the interaction of photons and that of charged particles. Photons can interact with matter via three different processes:

- **Photoelectric Effect:** This effect predominantly appears in the low energy range (1-100 keV) and is characterized by an atomic electron absorbing the total photon energy and gaining enough energy to become a free photoelectron. The resulting kinetic energy of the electron is given by $E_{el} = \hbar\omega - E_{bind}$, where E_{bind} is the binding energy of the electron and $\hbar\omega$ is the energy of the incoming photon. Since the electron can be excited from different shells, the absorption cross section varies stepwise.
- **Compton Scattering:** The photon and electron scatter elastically while energy and momentum are conserved. This process is dominant in an energy range between 100 keV and 1 MeV.
- **Pair Production:** If the photon energy is more than 1.022 MeV, i.e. twice the electron mass, an electron-positron pair can be created. To maintain energy and momentum conservation, the process must occur close to a nucleus [3], [4].

In atomic gases, the best range to detect photons is the near ultra-violet to hard X-ray domain, since higher energetic photons have low interaction cross sections with the gas [4]. For the ^{55}Fe test source used in this thesis, which decays by

2 Active Target Gas Detector

electron capture, followed by the emission of a 5.9 keV gamma ray, to ^{55}Mn , the dominant process that occurs is the photoelectric effect. The gamma ray represents hereby a Minimum Ionizing Particle (MIP).

When a charged particle passes through matter it will lose energy primarily by electromagnetic interactions with electrons and nuclei in the target material. Due to collisions energy is transferred to excite and ionize the atoms in the target material while the particle slows down. The average transferred energy per collision is small. The direction of the particle is changed by scattering from nuclei. The energy loss per unit length, or stopping power $\frac{dE}{dx}$, of a charged particle in matter is given by the Bethe-Bloch formula:

$$\frac{dE}{dx} = -\rho \frac{2KZ}{A\beta^2} \left[\ln \left(\frac{2mc^2\beta^2}{I(1-\beta^2)} \right) - \beta^2 - \frac{C}{Z} - \frac{\delta}{2} \right] , \quad (2.1)$$

$$K = \frac{4\pi N e^2}{mc^2} , \quad (2.2)$$

where β and I are given by the velocity and mean energy loss of the particle due to excitation, ρ , Z and A are the density, atomic number and mass of the medium, m and e are the mass and charge of the electron and N is Avogadro's number. The formula shows that the energy loss depends mostly on the particle's velocity [4]. The terms $\frac{C}{Z}$ and $\frac{\delta}{2}$ are added to take shell corrections and density corrections into account, respectively.

2.2 Drift and diffusion

In a gas detector, electrons and ions, created by photon or charged particle interactions, will start to diffuse due to statistic fluctuations and, if an electric field is applied, drift to the oppositely charged electrodes due to the electric force.

Without an electric field, the spread of charges after a diffusion time t follows a Gaussian distribution,

$$\frac{dN}{dx} = \frac{N_0}{\sqrt{4\pi Dt}} e^{-x^2/4Dt} , \quad (2.3)$$

where N_0 is the total number of charges, x is the distance from the origin and D is the diffusion coefficient. The standard deviation for linear and spherical diffusion is given by

$$\sigma_x = \sqrt{2Dt} \quad \text{and} \quad \sigma_r = \sqrt{6Dt} , \quad (2.4)$$

respectively. The velocity of a particle with mass m for a temperature T is given by a Maxwell distribution with an average speed of $v_T = \sqrt{\frac{8k_B T}{\pi m}}$, where k_B is

2 Active Target Gas Detector

Boltzmann's constant.

When an electric field is applied, electrons and ions are accelerated along the field lines. Since the acceleration can be interrupted by collisions, an average velocity is observed. This velocity is known as the drift velocity v_D of the charge. For ions, the drift velocity is low in comparison with v_T , while the electrons can exceed v_T due to their low mass. The resulting charge distribution is therefore drop shaped. Additionally, the drift velocity grows linearly with increasing electric field. Therefore, the mobility μ of a charge is defined as $\mu = v_D/E$ [4].

2.3 Avalanche multiplication

To observe reactions in a gas, the electrons which are produced by the processes described in section 2.1 are collected on the anode readout plane. Due to the applied electric field, the primary ionizing electrons are accelerated and undergo avalanche multiplication; if their energy is higher than the ionization potential of the gas, more electron-ion pairs are produced. These so called secondary electrons can also produce more electron-ion pairs if their energy is sufficient. Therefore, the number of electrons created by this process increases exponentially and produces avalanche, which is essential to detecting a measurable signal. The multiplication factor of an electron, passing a unit path length x through a gaseous environment, in a uniform electric field, is given by $M = e^{(\alpha x)} = e^{x/\lambda}$, whereby λ is the mean free path. The coefficient α , the first Townsend coefficient, describes the possibility to produce an electron-ion pair per unit length. It depends on the chosen gas and the applied field, E , and pressure, p . The normalized avalanche size is given by a Poisson distribution, for which the avalanche probability is given by

$$P(x, N) = \frac{x^{N-1}}{(N-1)!} e^{-x} \quad , \quad (2.5)$$

where N is the number of initial electrons and $x = n/\bar{n}$ the ratio between n , the exact number of electrons in a given avalanche, and \bar{n} , the mean number of electrons in one avalanche [4]. Figure 2.1 shows the probability distribution for different sizes of the avalanche depending on the number of initial electrons.

2.4 Penning and quenching effects

When a mixture of pure noble gas with a small percentage of a molecular gas is used, the so called Penning effect can increase the ionization process. Since the molecular gas has a higher ionization potential due to rotational and vibrational excited states, it can, if excited, transfer this energy in collisions to the noble gas, which is then ionized and a free electron is created. This can be described by the

2 Active Target Gas Detector

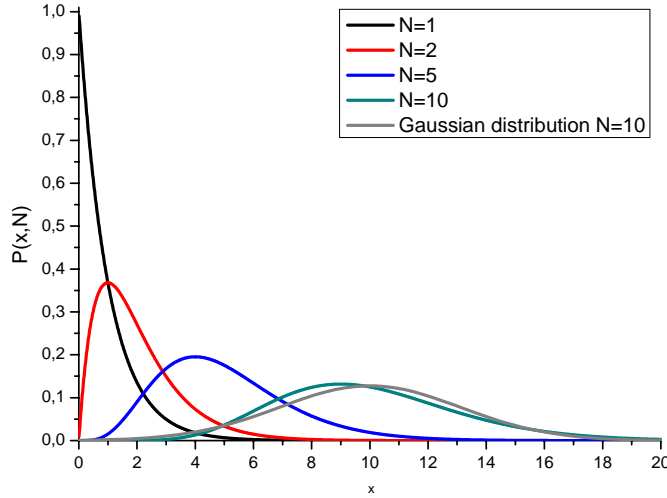


Figure 2.1: Normalized avalanche size probability for different number of starting electrons. The Gaussian distribution for $N=10$ is given by the grey curve.

following reaction formula.



The free electron can, as above, give rise to avalanche multiplication, which increases the detector gain. In this experiment a gas mixture of 82% Argon and 18% CO_2 was used. Moreover, the carbon dioxide also acts as a quencher, which prevents permanent avalanches, that can be caused by electrons, or photons released by ion recombination [4].

2.5 Proportional counter

Depending on the voltage that is applied between the cathode and anode in a gas detector, the amount of collected charge varies, which is shown in Figure 2.2a. The possible different operation ranges are labelled in the figure.

For very low voltages, the electron-ion pairs will recombine before they can be read out at the anode and cathode. In the ionization range, the voltage is high enough so that all charges are collected. The detector used in this thesis operates, like the first detectors which used the principle of avalanche multiplication, in the proportional counting region. As the name implies, in this region the collected charge is proportional to the number of primary electrons. The first proportional counters consisted of a gas filled cylindrical shaped cathode with an anode wire in its centre. When a high voltage is applied to such a configuration, the electrons produced by ionization drift towards the anode and undergo avalanche multiplication in the intense field close to the wire. Due to their low mass,

2 Active Target Gas Detector

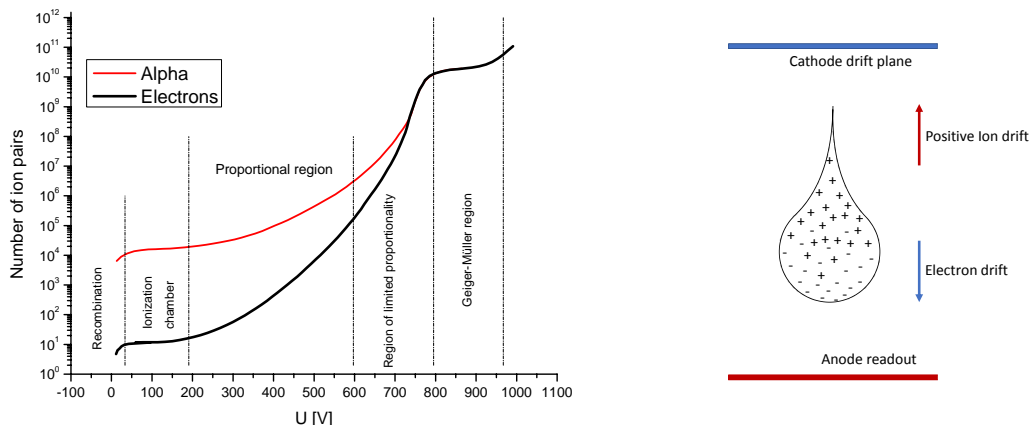


Figure 2.2: Left panel: Principle of avalanche formation. Due to the high mass of the ions, they drift slower towards the cathode. The resulting avalanche shape is drop-like. Right panel: The amount of ions collected for varying field strengths. The different operation ranges for gaseous detectors are shown. Data reproduced from [4].

the electrons reach the anode wire fast, while the ions drift slowly towards the cathode mantle. The avalanche is therefore drop shaped, as shown in Figure 2.2b.

For higher field strength the range of limited proportionality is reached, where the multiplication is large enough to cause distortions in the electric field around the anode wire. Finally, in the Geiger-Müller region every charge creates an equal signal due to continuous avalanches.

2.6 Gas Electron Multiplier

2.6.1 Operational principle

The electron amplification for the active target detector is realized using a Gas Electron Multiplier (GEM), a micro pattern gaseous detector. In this work, the GEM foils used consist of a thin Kapton foil of thickness, $T = 50 \mu\text{m}$, coated with, $t = 5 \mu\text{m}$, copper on each side. Small biconical holes with an inner diameter of $50 \mu\text{m}$ and an outer diameter of $70 \mu\text{m}$, with high density, go through the foil (see Figure 2.3a). The pitch, p , between the holes is $140 \mu\text{m}$ (see Figure 2.3b). When a voltage difference of a few hundred volts is applied to the different copper sides of the GEM foil, strong electric fields are created in the holes. Since the GEM foils are placed at the end of drift region, the electrons undergo avalanche multiplication in the holes, which act as independent proportional counters. The GEM foils will therefore reproduce the spatial distribution of the electrons that arise from an ionization track caused by a heavy ion traversing the gas.

2 Active Target Gas Detector

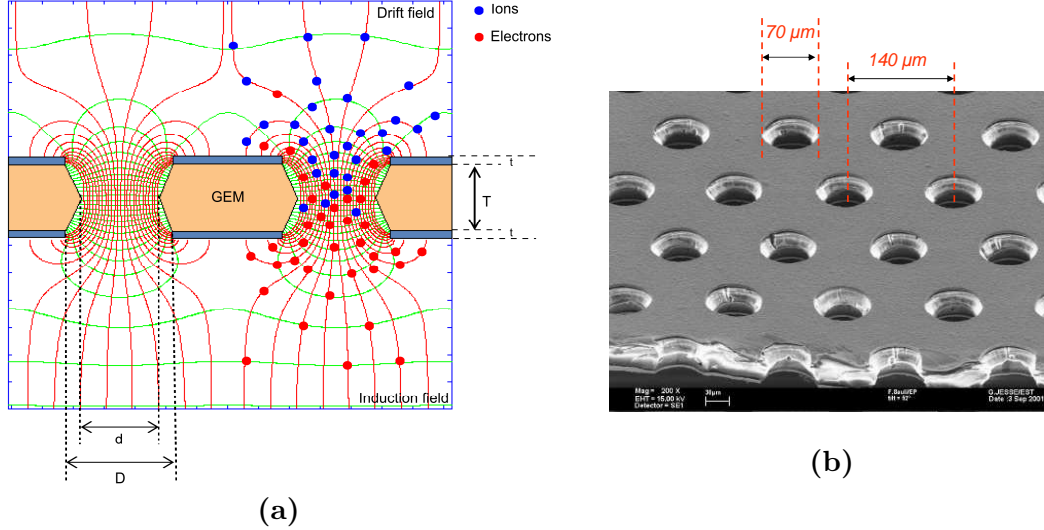


Figure 2.3: Panel (a): Detector principle of a GEM. Equipotential lines and example electrons \bullet and ions \bullet are marked (varied [6]). The thickness of the Kapton and the copper foil is $T = 50 \mu\text{m}$ and $t = 5 \mu\text{m}$, respectively; the inner and outer hole diameter $d = 50 \mu\text{m}$ and $D = 70 \mu\text{m}$ are drawn in. Panel (b): Photo of a GEM, pitch $p = 140 \mu\text{m}$ and outer hole diameter $D = 70 \mu\text{m}$ are marked [7].

Different types of GEM foils can be used depending on the application. In e.g. thick GEMs, the holes are burnt in the $\sim 600 \mu\text{m}$ thick Kapton foil by a laser instead of using the etching technique used for standard thin GEM foils [5]. Thick GEMs are very robust and have a high gain. In the beginning of GEM usage in 1990ies, GEMs were used in multiwire proportional chambers (MWPC) to increase the gain [4]. When later tests showed that GEM foils can produce enough gain without charge multiplication along the wires in the MWPC, the latter was omitted. GEM foils are very sensitive to dust since it can short-circuit the two copper plated sides via the holes and as a result damage the foil. Consequently the foils must be mounted and dismounted in a clean area.

In the detector setup of this thesis, there is a stack of three GEM foils. The electrons move through the holes in the foils, towards the anode, due to the electric field between two adjacent foils, and between the last foil and the anode. A signal can then be read out either after the last GEM foil, or after the readout plane. The setup with three stacked GEM foils is a standard setup. In this configuration the gain is high while the voltage over each foil is relatively low and breakthroughs are limited. To power the GEM foils, two different techniques were used in this work. In both cases, the voltage over the top GEM foil was

2 Active Target Gas Detector

chosen to be the highest with decreasing voltage down to the bottom foil. In the first tests a printed circuit board was used to apply the voltages. Here, the resistors were chosen in order to keep the voltage over the upper foil 10 % higher, and over the lower foil 10 % lower, than for the middle foil to prevent discharge [8]. For the second setup, the voltages were applied directly to the GEM foils to reduce the risk of sparking on the voltage divider.

Due to the high density of holes in the foil, the electron spread is not limited by foil characteristics, such as hole size and pitch, but by thermal diffusion. Moreover, the ions created in the holes, which could give rise to a bad timing resolution when recording the signal, are collected by the top sides of the GEM foils. The signals have therefore a small ion diffusion tail.

The geometry of the GEM foils is not important for the multiplication process. This is an additional advantage as it makes it possible to adapt the shape of the foils to different experimental applications. The usage of spherical shaped foils and non-planar detectors have become possible [7].

2.6.2 Gain

The effective gain of a GEM detector is given by the number of electrons, created by each primary electron, that reaches the read-out electronics. The produced current, I , is proportional to the product of the number of primary electrons, n_p , the gain of the detector G , the interaction rate, f^* and the electron charge e ,

$$I = e \cdot n_p \cdot f^* \cdot G \quad . \quad (2.7)$$

The interaction rate f^* can be derived from observing the count rate for different voltages. According to the operational principle of gas detectors described in section 2.5 not every electron produced is collected for low voltages. When the voltage is increased, the number of collected electrons grows. When the voltage is high enough and all electrons reach the readout plane, the detected count rate is limited by the interaction rate. As a result, a plateau in the count rate is reached. The gain, i.e. signal amplitude, will continue to grow for higher voltages but is finally limited by the maximum voltage the foils can sustain before breakdown.

The number of produced primary electrons, n_p , depends on the incoming radiation and the involved gas, and can be found in tables or from simulations based on known cross sections. Since the electron charge is known and the current can be measured, the gain can be determined. In principle, the size of the holes in the GEM foil also influences the gain. The smaller the hole, the higher the gain. This dependence is valid until a threshold of 70 μm [9]. Moreover, when the GEM is

2 Active Target Gas Detector

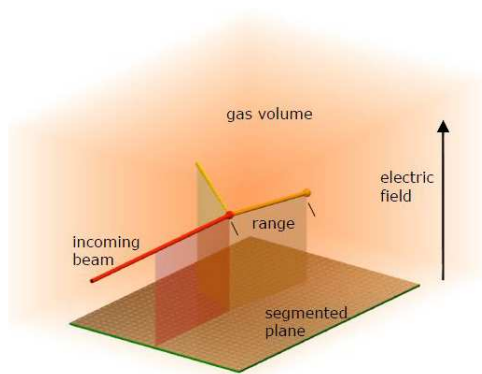


Figure 2.4: Principle of a TPC: reaction products produced by the collision of the incoming beam and the gas drift towards the anode while ions move towards the cathode. The drift time is used to construct the third dimension [6].

powered on it takes a while for the gain to stabilize due to charge that is deposited inside the holes. This charge polarizes the polymer and therefore influences the electric field in the holes and thus the electron multiplication. The influence of the charge up effect on the measurement increases with increasing difference in the the inner and outer hole diameter, since the insulator surface increases. The pitch of the holes does not influence the gain but the efficiency of the detector [9].

2.7 Time Projection Chamber

The detector in development here will in the end be used as a Time Projection Chamber (TPC). The final goal is to induce reactions in the drift volume and to reconstruct the reaction kinematics. In the laboratory this will in a first step be mimicked by inserting a radioactive source in the drift volume from which alpha particles and beta particles can be observed. The aim is to distinguish the detector response for these particles by detecting the read out signals via sampling ADCs. The schematic working principle of a TPC is shown in Figure 2.4.

The electrical signal, which is produced by the electron cloud after the avalanche, can be used to construct a two dimensional image of the track. When the drift time of the electron is measured, motion in the third dimension can be extracted as well. The measurement of the drift time can be done in several ways. The signal of an external detector can be used to start a time measurement that is ended by electrons reaching the readout plane. As an alternative, the internal time structure of the beam can be used for timing. A third possibility is to use internal triggering, where it is assumed that the first registered signal in the readout plane occurred along the beam axis. The time measured in this case is

therefore referred to as the time measured relative to the first interaction in the gas instead of given by an absolute start time.

2.8 Readout

The readout plane in this setup consisted of 256×256 strips in the x-y-plane read out via a Panasonic 130 pin connector (see Figure 2.5a). The signals could be added in groups of 128 signals to lemo0 connectors to readout and visualization on the oscilloscope. A backgammon shaped readout plane was also manufactured in order to investigate the signal spread in a future setup based on the simulations done in this work. In the future, backgammon shaped readout pads should be used. The segmentation of the anode is important to know where the electrons hit the readout plane.

In this thesis, two layers of separated strips in x and y direction are used for readout so that the position can be tracked when coincidences appear for a pair of x and y strips. The position resolution is therefore limited by the width of the strips and the coincidence timing for the electrode and the electronics [10]. The strips of the used readout plane have a width of $50 \mu\text{m}$ and a pitch of $350 \mu\text{m}$ (see Figure 2.5b).

In case of a non-segmented anode one could either use the relative propagation time of the signal, or the ratio of the collected charge at the corners of the readout plane can be used to find the hit position [11]. Other readout possibilities include pads, wedge and strip, or the backgammon shaped electrode. The method of choice here for future tests is a backgammon shaped electrode. Hereby, the plate is subdivided by saw tooth like narrow insulation gaps. When an electron avalanche hits the electrodes, the total charge will be subdivided between them. The different charges Q_1 , Q_2 , Q_3 and Q_4 , which are necessary to get two-dimensional position information, were historically obtained by connecting a charge divider to the wedge-shaped extension of the backgammon anodes (see Figure 2.6). For x and y information the following relations are then valid:

$$X \propto \frac{Q_1 + Q_2}{Q_1 + Q_2 + Q_3 + Q_4} \quad ,$$

$$Y \propto \frac{Q_2 + Q_4}{Q_1 + Q_2 + Q_3 + Q_4} \quad .$$

Today, the charges can be read out directly and processed by software.

During the first measurements, the signals from the readout plane were summed up and the current measured by a picoammeter via a LabVIEW interface. The signal was extracted from the bottom of the last GEM foil. To decouple the preamplifier from high voltage, a 1 nF capacitor was inserted between the foil

2 Active Target Gas Detector

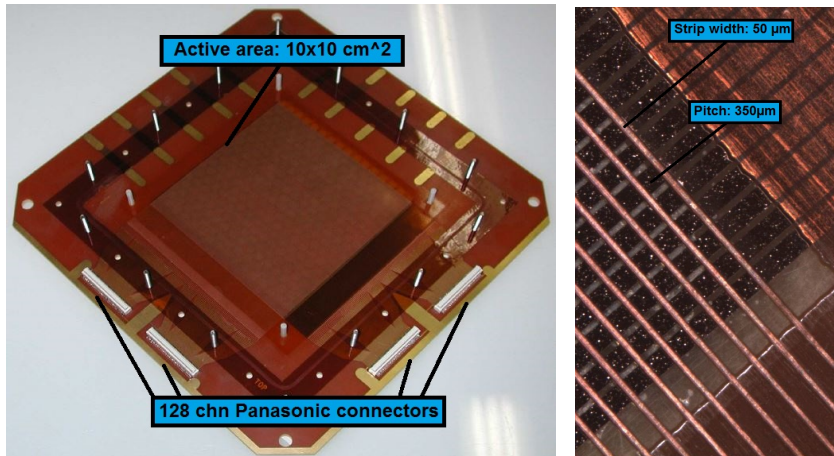


Figure 2.5: Left panel: Overview with two Panasonic connectors per dimension for readout. Right panel: Zoom on the readout plane to resistivity coupled strips in x- and y-dimension.

and the picoammeter via the voltage divider board. The signal was fed via a preamplifier to a Timing Filter Amplifier (TFA) and finally to a Multi Channel Analyser (MCA) that registered the pulse height and sent it to a laptop PC (see Section 3.2).

In the second set of measurements, the signal was extracted from the readout plane and fed into readout electronics provided by the ALICE group in the Particle Physics division in Lund. In this case, in order to provide a trigger signal, the signal was amplified by preamp and TFA, before it was connected to the readout electronics. The electronics consisted of up to 3 Front End Cards (FECs) connected to a Readout Control Unit (RCU). There is a back plane bus with 16 positions, to power and connect the FEC to the RCU. The signal from the readout plane is distributed to the FECs via Kapton cables fitted with Panasonic connector (type AXK5SA3277YG). An adapter card was designed to transfer the signal to the JEA40 Japan electronic adapters used on the FECs. A more detailed description of the setup is given in Section 5.

2 Active Target Gas Detector

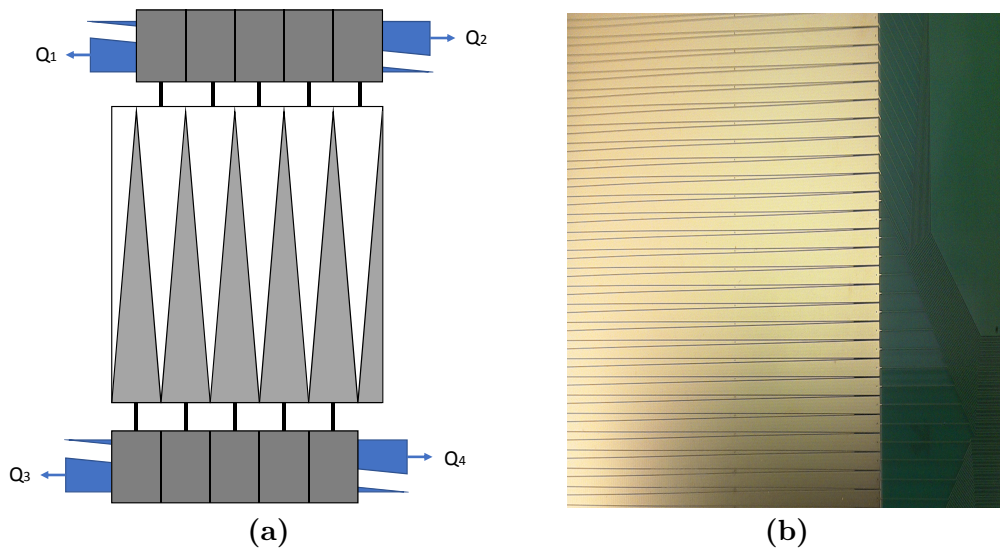


Figure 2.6: Panel (a): Principle of MBWC readout, Q_1 , Q_2 , Q_3 and Q_4 are used to reconstruct the hit position. Panel (b): Photo of backgammon readout plane built for future development of the GEM detector.

3 Measurements with GEM foils

3.1 Assembly

The assembly and test of GEM foils used in this work was done from scratch and foils were also replaced during the work. As mentioned in section 2.6, GEM foils are very sensitive to dust. Dust in the holes can short-circuit the two metal coated sides of the foil, which can lead to discharge and irreparable damage of the foil. Exposure to dust must therefore be kept at a minimum. As an alternative to using a clean room for the assembly work, as was done in earlier assembly work in this project, a clean fume hood in the chemistry laboratory in the Nuclear Physics Division was used instead. This approach has the advantage to give quick and easy access to a clean area for troubleshooting and configuration changes.

The test setup for the GEM detector developed in the project is based on a standard GEM detector kit from CERN. The GEM foils have an active area of $10 \times 10 \text{ cm}^2$ and are mounted on a 0.5 mm thick epoxy frame. The two sides of the active area are connected via fan connectors to pads on the readout plane where the bias voltage is supplied (see Figure 3.2a). The readout plane consists of 256×256 strips, as mentioned in section 2.8. The foils are mounted in a stack on nylon screws and the fans are soldered to connections on the readout board where the bias voltage is supplied (see Figure 3.2c). To obtain correct spacing between the foils, 0.5 mm thick spacers are inserted (see Figure 3.2f). The distance between the GEM foils, and between the last GEM foil and the readout plane was set to 2 mm. The drift region was 3 mm for the first setup, while it was raised to ~ 5 mm for later tests in an expanded gas volume using a gas tight Plexiglas box manufactured for the purpose. In the first measurements the gas volume was created by an epoxy frame with gas inlet and outlet (Figure 3.2b) and a Kapton gas window (see Figure 3.2d). To seal the volume, o-rings are inserted between the frame and the end plates. When the frame is mounted to the readout board, there is ca 1 cm distance on each side to the GEM foils (see Figure 3.2d).

Before new GEM foils are mounted in the gas volume, the foils have to be conditioned and their performance controlled. Firstly, a capacitance test is done. According to the data sheet for the GEM foils the capacitance of a foil should be $\sim 5.8 \text{ nF}$. Secondly, the foil is examined for discharges by applying a voltage

3 Measurements with GEM foils

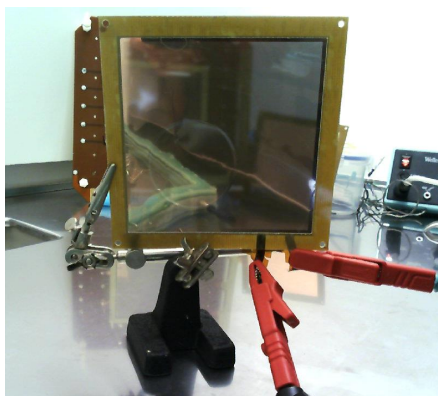


Figure 3.1: Current test of a new GEM foil. The voltage is applied via the fan connectors.

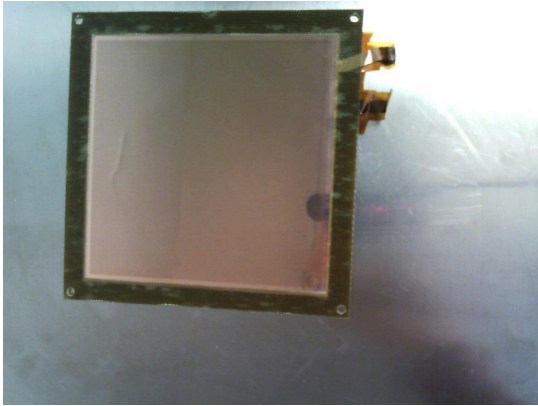
Table 3.1: Capacitances and leakage currents of the used GEM foils

Position	Leakage I [nA]	Capacity [nF]
top	3	5.67
middle	2	5.71
bottom	2	5.69

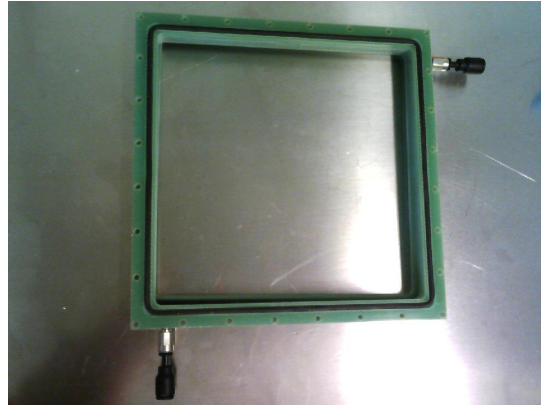
of about 600 V for one minute. If the current stays below 10 nA, the foil passes the test. A picture of the voltage test of a new foil is shown in Figure 3.1. The foil is mounted in a vertical position during the test to minimize the amount of dust falling on the active area.

During the first weeks, the foils used in the previous work were exchanged due to damages. Before new foils were used in the detector, they were examined visually, the capacitance and leakage current were tested, after which they were stacked and soldered to the readout board following the procedure outlined above.

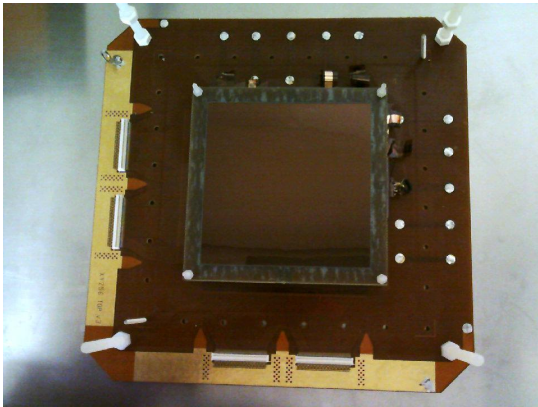
3 Measurements with GEM foils



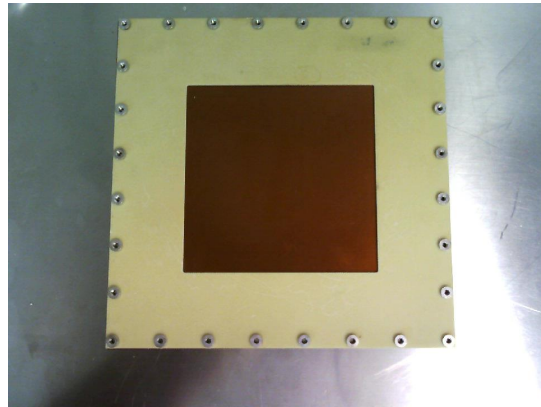
(a) GEM foil with fans



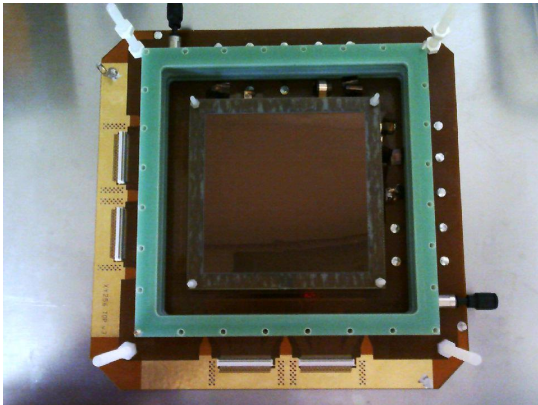
(b) Epoxy frame with gas inlets



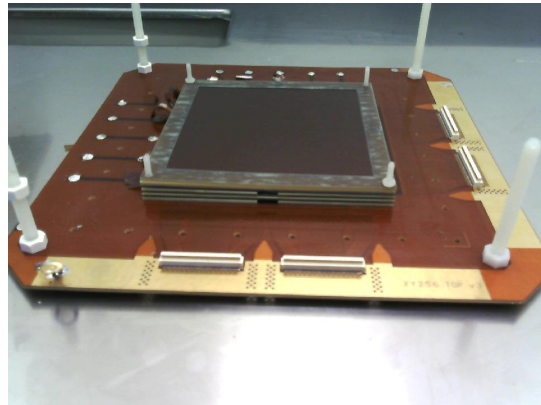
(c) Mounted GEM foils



(d) Kapton window to let radiation in



(e) Mounted GEM foils with frame



(f) Mounted GEM foils - sideview with spacers

Figure 3.2: Assembly of the GEM detector.

3.2 Setup

Two different setups were used to supply bias voltage to the GEM foils and produce the drift voltage needed to get the electrons to drift through the detector. In the first measurements a voltage divider consisting of a resistor chain was used to apply voltage to the foils. A circuit diagram of the voltage divider is shown in Figure 3.3. The resistors were chosen to have resistances of 550, 500 and 450 k Ω , in a configuration that decreases the voltage from the topmost to the bottom-most foil to prevent discharges as mentioned in section 2.6. The detector itself was placed in a metal box for grounding and to reduce noise pick up. A picture of this setup is shown in Figure 3.4.

As is shown in Figure 3.3, 10 M Ω resistors are connected between the voltage divider and the top sides of each GEM foil. This is done in order to protect the foils if a short circuit occurs in one of them. Due to the parallel connection of the resistor across the foil, with a resistance \sim 500 k Ω (R_1), and the 10 M Ω resistor (R_2), the voltage drop across the resistor will not differ significantly from the value before the short circuit. This can also be seen from the well-known relationship for two resistors connected in parallel.

$$R_{tot} = \frac{R_1 \cdot R_2}{R_1 + R_2} \stackrel{R_2 \gg R_1}{\approx} \frac{R_1 \cdot R_2}{R_2} = R_1 \quad (3.1)$$

The short circuited foil will thus approximately maintain the potential that the lower copper plated side had before the breakthrough.

The signal for the following measurement was taken from the end point of the voltage divider, which was connected to the bottom of the last GEM foil. A capacitor of 1 nF was used to decouple the preamplifier from the high voltage. The signal for the current measurement was taken directly from the readout plane. The signals strips of the readout plane were summed for these measurements. It is important to notice that the signal from the bottom of the last GEM foil and the signal from the readout plane are equal except of the sign.

For the second setup, the voltages were applied directly to the GEM foils to reduce sparking on the voltage divider. The signals were in these measurements taken from the readout board. For shielding purposes, to reduce noise, the detector was first placed on a metal plate and later inside a metallic mesh in order to create a Faraday's cage inside of the gas tight Plexiglas box. The power supply used with the first setup was a CAEN N470, and the second a CAEN SY127.

To generate a signal, a ^{55}Fe source was placed on the Kapton window. The read out signal was amplified by a Ortec 142 preamplifier and a Canberra 2111 timing filter amplifier (TFA). The amplified signal was fed to a multi channel analyzer

3 Measurements with GEM foils

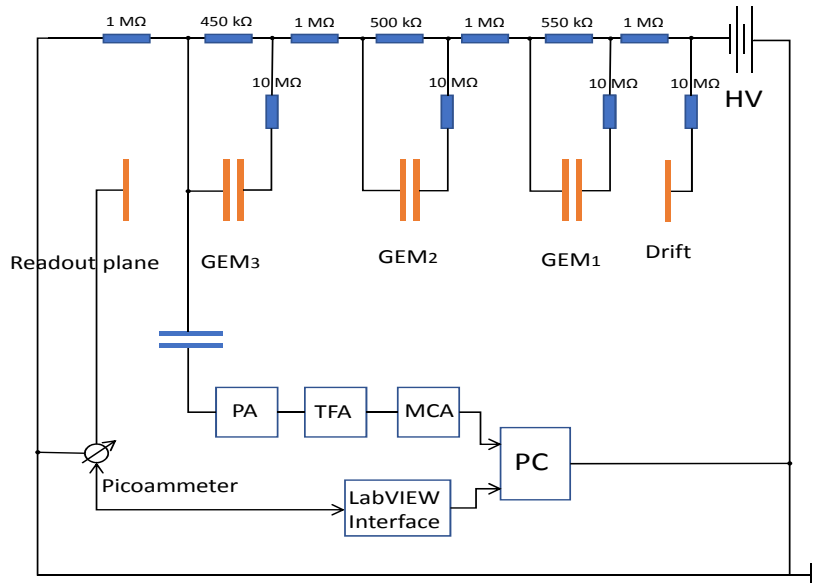


Figure 3.3: Circuit diagram of the voltage divider and the measurement setup.

(MCA), connected via USB to a PC. The current was read out by a Keithley 6487 picoammeter and processed via LabVIEW over a GPIB interface. The TFA was set to 20 ns differentiation, 500 ns integration, a coarse gain of 100 and fine gain of 2.

3.3 Rate and gain

3.3.1 Voltage divider

After a change of GEM foils, the first step is to measure the gain, and control whether the gain expected from previous work, is reached. In this case the measurements were compared to the results in Ref. [2]. Previous tests involved measuring gain for different gas mixtures but as this work has an increased scope, performance was compared only for one gas mixture with 82 % Argon and 18 % CO₂. The voltages that were applied are shown in Table 3.2.

The gas flow was controlled with a flow meter and set to ~ 8 l per hour. After the source was applied, the number of registered events was measured with the MCA, applying a threshold at channel 225. Four spectra were taken for each voltage using a measurement time of 30 seconds. Two spectra were recorded with, and two without the source. For the background measurements the source was moved to a sufficient distance from the detector to avoid events arising

3 Measurements with GEM foils

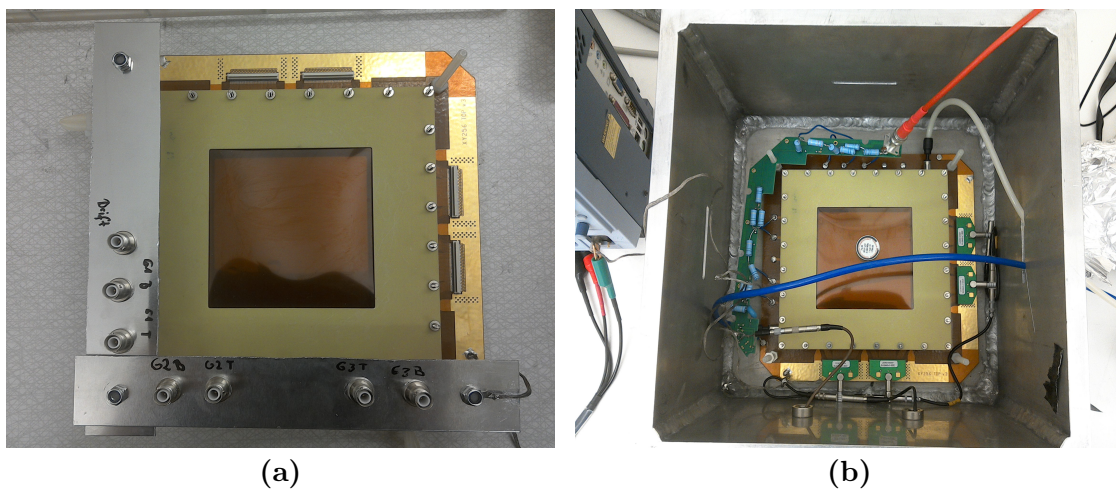


Figure 3.4: Panel (a): Completely assembled GEM detector with direct voltage supply without connection to gas, HV and readout connector. Panel (b): The detector with voltage divider board in metal box; HV, readout cables and gas are connected. The source is placed in the centre of the Kapton window.

from scattered photons entering the sensitive volume. In Figure 3.9, spectra for 3800-4050 V total drift voltage are shown, whereby the appearance of the Argon escape peak is observed.

The rate curve for the 82/18 Ar/CO₂ gas mixture is shown in Figure 3.5. The measurements were fitted using the following model:

$$y = \frac{a}{1 + \exp(-b(x - c))} \quad , \quad (3.2)$$

where a gives the count rate at the plateau, b the slope and c the saddle point of the slope. The plotting and the fitting were done using Origin 7.5. The rate at the plateau, at a flow of 8 l/h, was determined to be

$$f^* = 3644.1 \pm 28.4 \text{ Hz} \quad ,$$

where f^* corresponds to the interaction rate in equation 2.7. The saddle point appears around 3750 V. This value for f^* varies significantly from the one obtained in previous measurements in [2], $f^* = 963.2 \pm 37.8$ Hz. The saddle point from the earlier work, which sits at ~ 3700 V, is compatible with the value from this measurement. A possible reason for the rate difference, i.e. the higher efficiency deduced from the current measurements, can be the increased flow (earlier a flow of 4-5 l/h [2] was used) and potentially that gas leaks existed in the chamber earlier. This could lead to the gas volume not being completely filled with the correct gas mixture. There were no induction of reduced efficiency due to imperfections in the foils during the previous measurements, but the use

3 Measurements with GEM foils

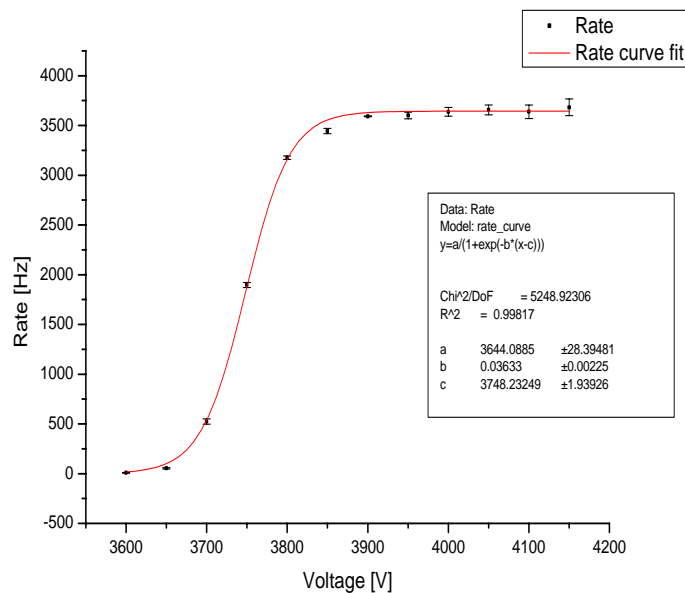


Figure 3.5: Rate curve for the 82/18 Ar/CO₂ gas mixture. Charge collection starts at a total voltage of ca 3.7 kV and reaches a plateau at ca 3.9 kV when all events occurring in the sensitive volume give rise to a signal on the readout plane.

of new and therefore ideally undamaged GEM foils may potentially also be a reason for higher efficiency.

The current was measured while changing the voltage from 0 to -4150 V. For the measurement with the source this creates the series of steps visible in Figure 3.6a. The measurement without source shows spikes in the current for changes in the high voltage (see Figure 3.6b). Nevertheless, the amplitudes of the spikes in the measurements without source are about one order of magnitude lower than the values from the measurement with the source.

To calculate the gain G , equation 2.7 can be rearranged to give,

$$G = \frac{I}{e \cdot n_p \cdot f^*}. \quad (3.3)$$

The number of primaries, n_p , has to be obtained from simulations based on known cross sections, the electron charge, e , is known and the rate, $f^* = 3644.1 \pm 28.4$ Hz was determined above. To extract the current, I , the measured current is averaged and the background subtracted for each voltage. The number of primaries, $n_p = 214.7 \pm 6.34$, was taken from simulations for the 82/18 Ar/CO₂ gas mixture in Ref. [2]. In section 4.2 the simulation procedure to obtain n_p is described briefly. The error for the gain ΔG was calculated employing error propagation using the

3 Measurements with GEM foils

Table 3.2: The voltages applied across different parts of the GEM detector using the voltage divider setup. At an operating voltage of 3900 kV, the voltage over the 3 mm thick drift volume is 681 V, and the maximum GEM bias voltage is 369 V.

Tot. voltage [V]	ΔV_{Gap}	ΔV_{GEM_1}	ΔV_{GEM_2}	ΔV_{GEM_3}
-3600	620	341	311	281
-3650	629	346	314	283
-3700	637	350	318	289
-3750	646	355	323	291
-3800	656	359	327	296
-3850	664	365	332	298
-3900	672	369	334	304
-3950	681	375	341	306
-4000	689	381	346	311
-4050	698	384	349	314
-4100	707	388	354	320
-4150	716	393	358	322

following equation,

$$\Delta G = \frac{\Delta I}{e \cdot n_p \cdot f^*} + \frac{\Delta n_p \cdot I}{e \cdot n_p^2 \cdot f^*} + \frac{\Delta f^* \cdot I}{e \cdot n_p \cdot (f^*)^2}. \quad (3.4)$$

The spectrum taken at $V = 4000$ is shown in Figure 3.8a. The spectrum is fitted with a double Gaussian to extract the rate of photopeak events. The smaller peak on the left side of the spectrum shows the Argon escape peak, while the larger peak is the full energy peak.

Since the charge up effects, discussed in section 2.6.2, stabilize after a certain time, a long term measurement was done for about 6 h with the voltage divider setup, to see how the detector behaviour changes over time. The gain was measured for a total voltage difference between drift and readout plane of $U = 3800$ V. The relative gain, obtained by dividing the measured the current by the mean current from the first 30 measurement points, is plotted versus the measurement time in Figure 3.10a.

The gain stabilizes after ca 5 hours at ~ 1.95 times the initial value. The signal as recorded on the LeCroy WaveSurfer 454 oscilloscope after the two amplification stages is shown in Figure 3.10b. The bipolar output from the TFA is used. The Argon escape peak can be seen at approximately half the amplitude of the 5.9 keV full energy peak. The escape peak arises from events where the 5.9 keV X-ray

3 Measurements with GEM foils

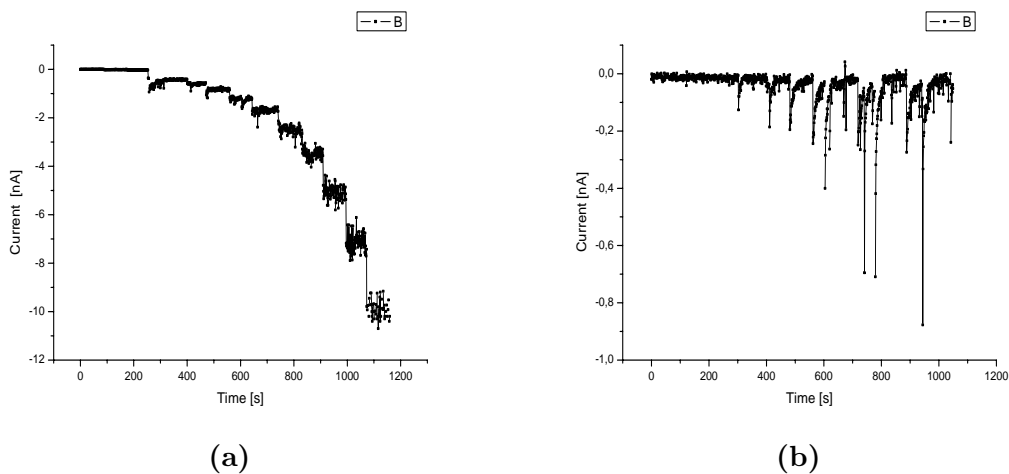


Figure 3.6: Panel (a): Measurement with source. The current increases stepwise as the voltage difference is increased (see text for discussion) Panel (b): Measurement without source. Spikes are seen in the current when the voltage difference is increased but the amplitude is ca one order of magnitude smaller than the current registered with the source. The background current returns to zero over the measurement period, while for the measurement with source it remains constant.

kicks out an electron from the K-shell in an Argon atom (binding energy ca 2.9 keV) and the X-ray, that is emitted as the vacancy is filled, leaves the sensitive volume without interacting further.

3 Measurements with GEM foils

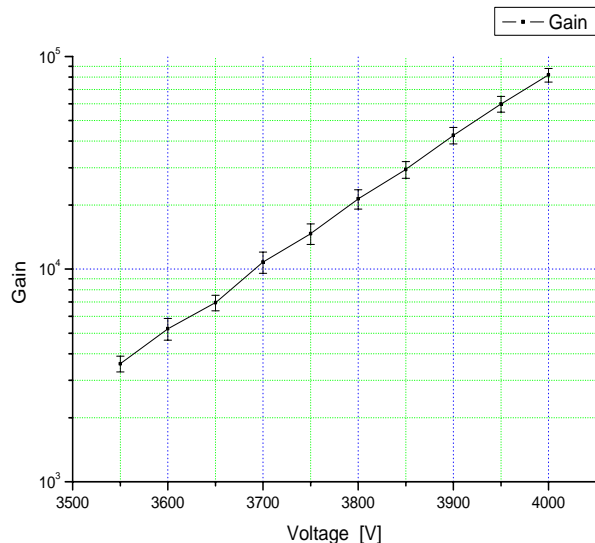


Figure 3.7: Gain curve for the 82/18 Ar/CO₂ gas mixture. A gain of $\sim 4 \times 10^4$ is obtained for a typical operation voltage of 3.9 kV and reaches a maximum of $\sim 8 \times 10^4$ at 4.0 kV

3.3.2 Direct voltage supply

In order to provide more flexibility when selecting the voltages over the GEM foils, and as a preparation for increasing the drift volume, i.e. the sensitive volume of the detector, a setup with individual bias for the foils and the drift volume was also tested. This setup made it possible to vary the voltages compared to the standard voltage setting using the voltage divider. Consequently, in this case the applied voltages differed from the ones in Table 3.2. The aim of this measurement was to find out the minimum electric field needed in the drift volume in order to observe the full energy peak. The voltage between the top drift plate and the readout plane was changed in the measurement, while maintaining the same setting for the GEM foils. As the Argon escape peak could be clearly observed for a total voltage difference between drift and readout plane of 4000 V with the voltage divider setup, GEM foil settings, ΔV_{GEM} , of 310 V, 345 V and 385 V for the low, middle and upper foil, respectively, were selected for the measurement. The voltages were then varied to obtain the electric fields according to Table 3.3.

The rate curve for the measurement is given in Figure 3.11a. Data were taken down to a drift field of 200 V/mm as the Argon escape peak could not be observed below this field. For the rate measurement, the value at the plateau, $f^* = 3711.1 \pm 23.6$ Hz, is consistent with the rate measurement in section 3.3.1. Since the signal was taken from the readout plane, the current was not measured with the picoammeter, but approximated using the currents obtained from the voltage

3 Measurements with GEM foils

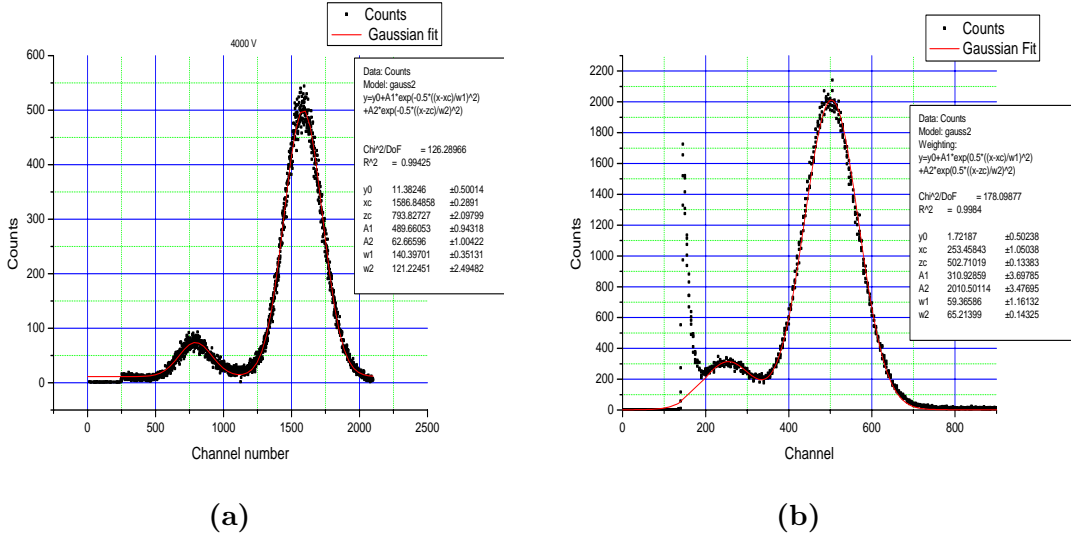


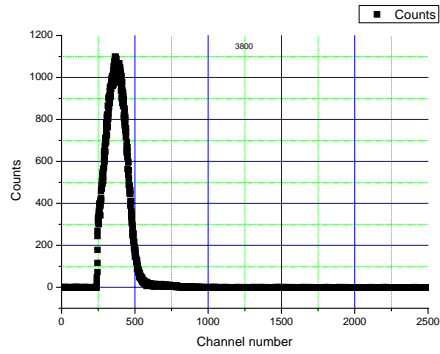
Figure 3.8: Panel (a): Spectrum at 4 kV using the voltage divider setup. Panel (b): The spectrum for a 345 V/mm drift, using the direct voltage supply setup.

divider setup for the same rate. The estimated gain curve is shown in Figure 3.11b. The spectrum for the 345 V/mm drift field is shown in Figure 3.8b. The Argon escape peak is partly hidden by the noise in the first channels. The larger number of counts in this spectrum, compared to the measurement using the voltage divider, is due to a longer measurement time.

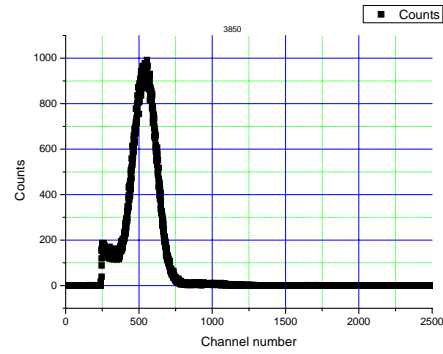
Table 3.3: Direct voltage supply setup: Voltages across different parts of the GEM detector.

V/mm	345	325	300	275	250	225	200
GEM _{3,bot}	690	650	600	550	500	450	400
GEM _{3,top}	1000	960	910	860	810	760	710
GEM _{2,bot}	1690	1610	1510	1410	1310	1210	1110
GEM _{2,top}	2035	1955	1855	1755	1655	1555	1455
GEM _{1,bot}	2725	2605	2455	2305	2155	2005	1855
GEM _{1,top}	3110	2990	2840	2690	2540	2390	2240
Drift plate	4145	3965	3740	3515	3290	3065	2840

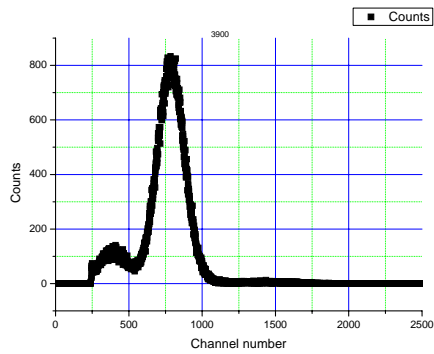
3 Measurements with GEM foils



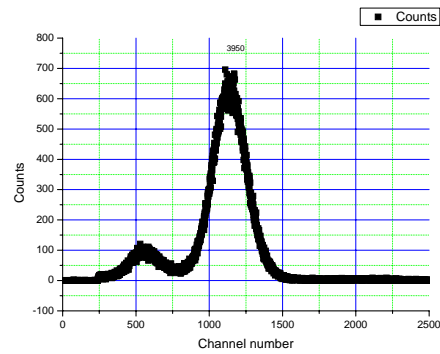
(a) 3800 V



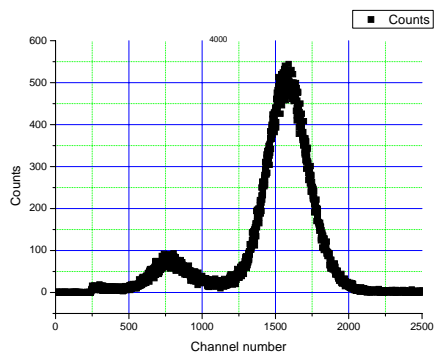
(b) 3850 V



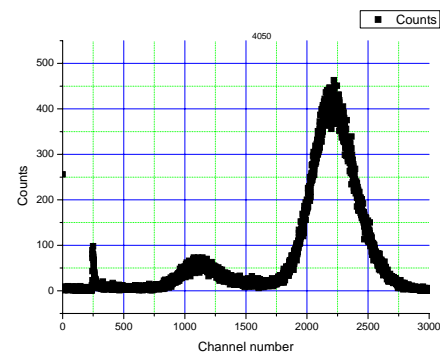
(c) 3900 V



(d) 3950 V



(e) 4000 V



(f) 4050 V

Figure 3.9: Spectra for different voltages. The higher the applied voltage is, the more the spectrum is shifted to the right.

3 Measurements with GEM foils

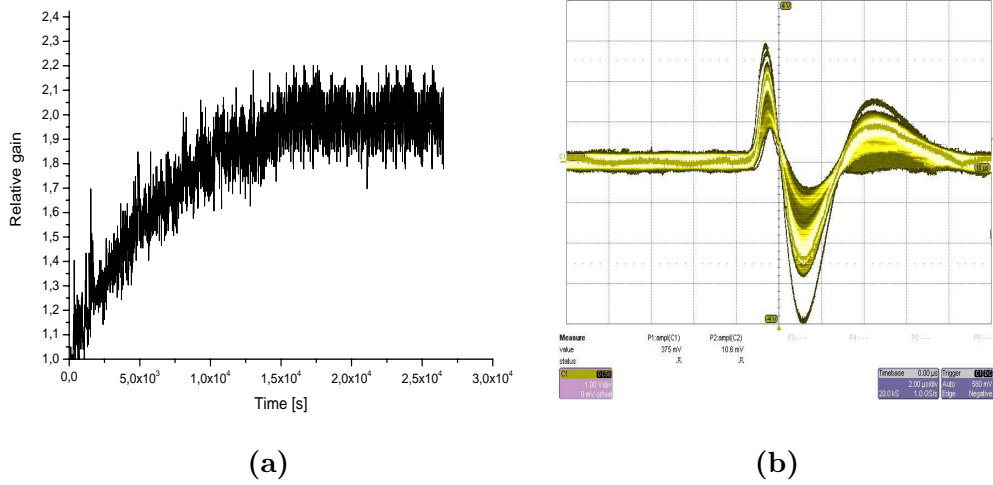


Figure 3.10: Panel (a): Relative gain for long term current measurement. Panel (b): Signal after amplification using the TFA bipolar output. The Argon escape peak can be seen at approximately half the amplitude of the full energy peak.

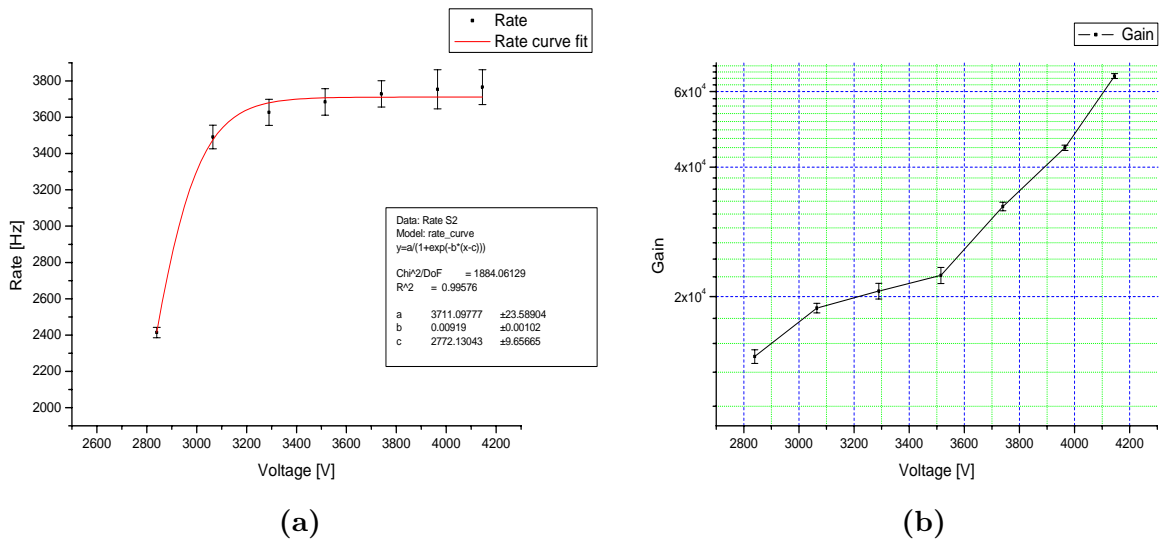


Figure 3.11: Rate curve measurement and gain curve estimation for the 82/18 Ar/CO₂ gas mixture. Panel (a): Rate curve measurement for the direct voltage supply setup. Panel (b): Gain curve estimation.

4 Simulation

4.1 Simulation Procedure

In the previous section the gain that can be accomplished with a stack of three GEM foils was investigated in different configurations. In the second measurement the drift field was varied in order to find the minimum field for which the argon escape peak was still visible in the spectrum. In addition to this information, which tells what voltage will be needed for a certain length of the drift space, it is also interesting to investigate the size of the electron cloud as it hits the readout plane. The size of the cloud will determine the precision with which the track can be reconstructed and will also guide when designing the readout plane, particularly when it comes to the size of the readout pads or strips. As a first step to investigate this in practise simulations were carried out as part of this work.

The simulations were performed with the ROOT based software Garfield++ [15], which is a simulation package for simulations of gaseous detectors. The program can be used to simulate the number of primary created electrons in the drift volume, the avalanche process and the gain of the detector, the read out signal, the size of the electron cloud when it reaches the anode wires and much more. It can also be used for constructing simple electric fields. However, since a GEM foil electric field is rather complex, an external solver, the finite element program Elmer [14], was applied for field construction. This finite element solver requires a mesh of the given geometry, which is provided by the program gmsh [13]. In the following sections, the simulation procedure and the obtained results are presented.

4.1.1 gmsh

In the first step, the detector geometry, in particular the GEM foils, is modelled in gmsh. Since a GEM foil is symmetric, the use of two quarters of the holes through the foil is sufficient to get the detector geometry for the field calculation. This also reduces the number of calculation steps. To simplify the calculation further, the drift region, which was varied in the simulations to investigate the electron spread as a function of the drift distance, at different pressures, was separately built in gmsh and the field calculated in Elmer.

4 Simulation

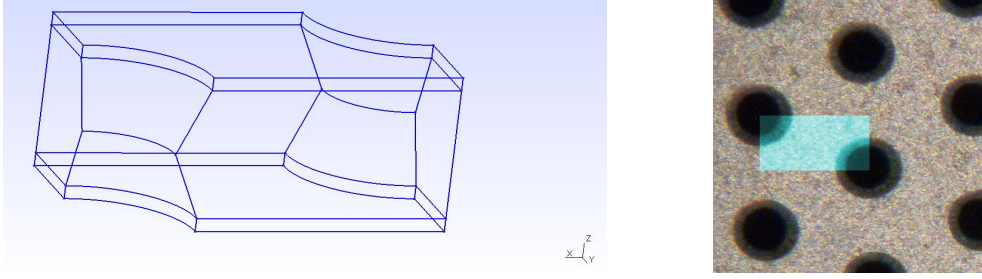


Figure 4.1: Left panel: The gmsh reconstruction of a GEM foil section used in this work. Three GEM foil sections were stacked over each other with a distance of 2 mm and mirrored to cover the full active area. Right panel: Corresponding area on real GEM foil.

The model of the GEM stack of in detector was constructed with a 3 mm drift region between drift cathode and the top of the upper GEM foil, and with 2 mm between the GEM foils and the last foil and the readout plate. As on the real GEM foils, a hole pitch of $p = 140 \mu\text{m}$, an inner hole diameter of $50 \mu\text{m}$, an outer hole diameter of $70 \mu\text{m}$, a copper thickness of $5 \mu\text{m}$ and a polymer layer thickness of $50 \mu\text{m}$ were used for the built geometry. One GEM foil layer is shown in Figure 4.1a.

To built the whole detector in gmsh, three GEM foil sections were set over each other with a distance of 2 mm. A plane for the readout was added in a distance of 2 mm and a plane for the drift in a distance of 3 mm. The setup was then mirrored in x and y direction to cover the full active area.

4.1.2 Elmer

Elmer is an open source software, that can be used to solve the electric field equations for the GEM. The required mesh is produced in gmsh and solved in Elmer via the Finite Element Method (FEM). FEM is a numerical method, for which the body is divided in smaller sub elements, the finite elements, which are interconnected by nodes. Since the electric potential ϕ of the GEM is static, Laplace's equation is valid as a special case of Maxwell's equation in charge free space:

$$\nabla^2 \phi = \nabla E = 0 \quad (4.1)$$

The elements can have any shape. The simplest is a tetrahedron with a node in each corner. Garfield++ works with second order elements, which have additionally a node in the middle of each connection line [14].

To solve the equation, the potential ϕ is approximated for every node section by basis functions ϕ_i , which are often polynomial functions. The differential equation is then written in its weak form, so that the solutions fulfil the equation

4 Simulation

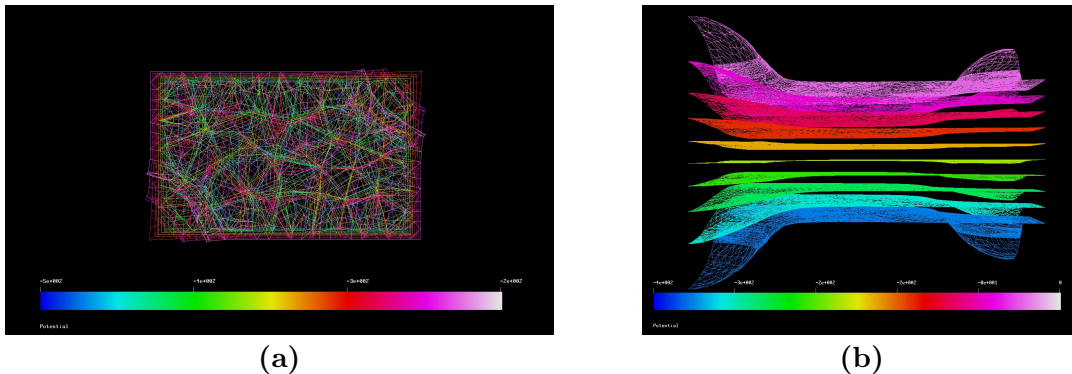


Figure 4.2: Elmer output for the GEM foil section. Panel (a): Mesh structure of electric field over GEM foil section. Panel (b): Calculated equipotential surfaces for the GEM foil section.

not absolutely but approximately. The potential is therefore replaced by a sum of linear equations:

$$\phi \approx \sum_{i=1}^n A_i \phi_i \quad , \quad (4.2)$$

where n is the number of nodes and A_i are approximated weighting functions. By inserting boundary conditions, the weighting functions are derived and the system is solved at the node values.

In Figure 4.2a, the mesh is visualized for the top sight of a GEM foil section. The different colours show the isosurfaces for a potential of -400 V over the GEM. A side view of these equipotential planes is shown in Figure 4.2b. The results in Figure 4.2b, for the equipotential surfaces compare well to the expected behaviour known from previous publications (see section 2.6, Figure 2.3a), The surface is almost planar in the central parts, while at the edges the field bends symmetrically.

4.1.3 Garfield++

Garfield++ is a simulation package, which was constructed explicitly to reproduce physical processes in gaseous detectors. Since the electric field of a GEM is not simple enough to be constructed via Garfield++, the field obtained by the Elmer is applied to the program. This can either be done using a Graphical User Interface (GUI) or by giving the path to the saved field during the execution. To calculate the properties of gas mixtures and the electron transport at a given electric field, Garfield++ uses the packages Heed and Magboltz. Magboltz calculates e.g. diffusion properties such as drift velocity and Townsend coefficient. The avalanche and the electron distribution are thereby calculated microscopically [15]. Since the avalanches are studied on the molecular scale, not only the

4 Simulation

starting electron, but also every electron created in the process, can be tracked. Garfield++ was used to calculate the gain of the detector (for which the Penning effect was taken into account), to estimate the amount of primary produced electrons in the drift volume, and to look at the induced signal. The electron cloud size and momentum at the readout plane were also simulated for different pressures using an electron starting position of 3 mm over the top GEM foil. The spread of the electron cloud from the drift plane to the top of the first GEM foil was also simulated in this thesis for different drift distances, drift voltages and pressures. The temperature was set to $T=20^\circ$ in the simulations and the gas mixture was 82/18 Ar/CO₂.

4.2 Number of primaries, gain and signal

The result of the previous and following chapters partly rely on previous simulations [2] that were revisited and used in this work. The simulation procedure and these results are briefly presented in this section.

The number of primaries is mainly needed to calculate the detector gain, as mentioned in section 2.6.2. Since the ⁵⁵Fe source decays by electron capture followed by the emission of a 5.9 keV gamma ray to ⁵⁵Mn, 5.9 keV photons were simulated in earlier work in a gas volume of $0.3 \times 20 \times 20$ cm³. The simulation was done with 10 million photons for three different gas mixtures. For this work only the 82/18 Ar/CO₂ mixture is relevant. The two peaks of the experimental spectrum, with full energy peak and argon escape peak were reproduced, as expected. The resulting number of primaries were 214.7 ± 6.34 for the full energy peak and 99.27 ± 4.58 for the argon escape peak [2].

For the gain, the number of electrons that reach the readout plane was obtained for different voltages. The Penning coefficient for the specific gas mixtures was taken into account for the simulation. When the number of primary produced electrons was injected in the gas volume, a Gaussian distribution was obtained for the avalanche size. For the 82/18 Ar/CO₂ gas mixture, a gain of 15000 was obtained for a total voltage of 4 kV.

The signal, which is induced on the readout strip j , can be calculated according to the Shockley-Ramo theorem,

$$i_j = -q\vec{v} \cdot \vec{F}_j \quad (4.3)$$

where i_j is the current induced on electrode j , q and \vec{v} are charge and velocity of the particle and \vec{F}_j the weighting field. The weighting field is obtained by the following equation: $\vec{F}_j = -\nabla V$. V is the weighting potential, which is calculated by Elmer with changed boundary conditions [14].

4.3 Electron spread

To simulate the spread of the electron cloud, the avalanches were tracked with the built in microscopic transport and avalanche method in Garfield++. The Penning coefficient was set, for the used gas mixture of 82/18 Ar/CO₂, to 0.53 [16]. The calculation of the spread was divided in two parts: the spread over a certain drift region before the particle enters the GEM detector, and the spread while traversing the GEM foils themselves. This has the advantage that the time to perform the simulation is decreased. Moreover, it can be estimated whether the spread is mostly influenced by the avalanche or by the diffusion during drift.

Consequently, both the avalanche size and the diffusion from the drift for the starting electrons were taken into account in this way. A typical cloud is plotted in Figure 4.3a. The width of the electron distribution on the readout plane after an avalanche, with only a short drift length, is ~ 1.2 mm on average. For the simulation of the multiplication in the GEM foils two different settings were used. In the first one the total voltage between the drift plate (the anode) and the readout plane was -3800 V. The voltages over the GEM foils were set to 380, 345, and 310 V, respectively, with a drift voltage of 690 V. For the second setting the voltage on the drift plate was changed to -4145 V while maintaining the same voltages over the GEM foils. These two settings correspond to drift fields of 345 V/mm and 230 V/mm. Only small differences in cloud dispersion was observed for the two cases.

To investigate the effect of different drift lengths on the cloud the drift distance was varied between 3 cm, 10 cm, 15 cm, 20 cm and 30 cm. The applied voltage on the drift anode was set to 8 kV for these cases. The pressure was also varied between 1, 3 and 5 bars for the 8 kV case. In each simulation, 1000 electrons were injected close to the drift plane and the cloud distribution was extracted 3 mm above the first GEM foil.

Due to diffusion, the electron cloud has a Gaussian distribution in the x and y directions. To quantify this spread, a Gaussian was fitted in the xy-plane and the standard deviations, σ_x and σ_y , were extracted as function of the drift distance, the applied potential and the pressure. In Figure 4.3b, the result for the electron cloud distribution for a drift length of 3 cm is shown at a total voltage of -8 kV, and a pressure of 1 bar. For these parameters the Full Width Half Maximum ($\text{FWHM} = 2\sqrt{2 \cdot \ln(2)} \cdot \sigma$) of the cloud is 1.1 mm. At six standard deviations, containing 99% of the number of electrons, the cloud is 2.5 mm wide. Consequently, the diffusion during the drift is comparable to the spread that occurs during multiplication also for a short drift length of 3 cm. The results for the 3 cm drift length at varying pressures is shown in Figure 4.4. It is clear that the width of cloud is reduced with increasing pressure. Consequently, operating the detector at higher pressure, to increase target thickness in an experiment, should not lead to reduced position resolution. The same trend concerning the

4 Simulation

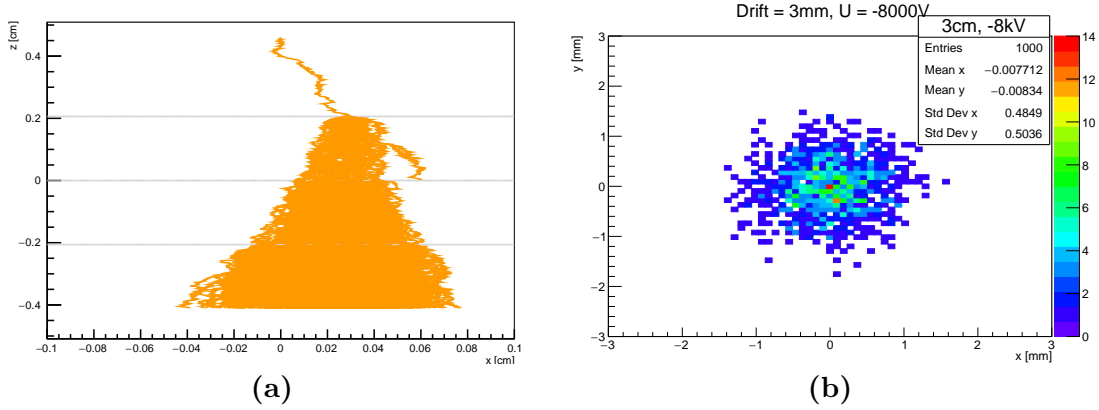


Figure 4.3: Panel (a): An avalanche of a single electron in 82/18 Ar/CO₂ mixture. The applied voltage over the detector was 3.8 kV. The electron tracks are plotted in orange, the foils in grey. Panel (b): Spread of 3 cm drift length, pressure $p = 1$ bar, $U = -8$ kV.

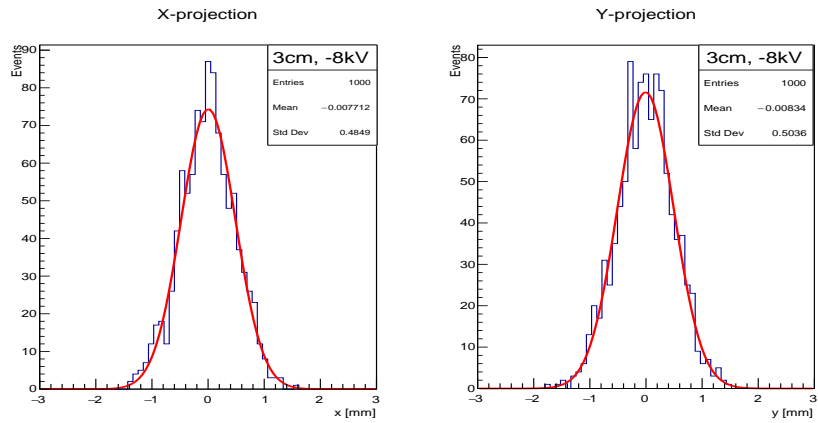
influence of pressure can also be observed for longer drift distances (see Figure 4.5a). As can be seen in the same figure, the size of the cloud also increases monotonically with drift distance. For the 1 bar case the FWHM increases from ~ 1.1 mm, as mentioned, to ~ 2.2 mm with a corresponding 6σ width of 5.6 mm at 1 bar.

The decreasing spread for increasing pressure can be understood by the more frequent collisions that occur with the gas atoms as the cloud diffuses in the xy -plane. The mean free path becomes shorter for the electrons, so that the variations in the xy -direction become smaller. The electron spread is therefore influenced by the amount of collisions with gas atoms, which depends on the applied pressure and the surrounding volume. Moreover, as discussed above the applied voltage influences the cloud spread. Thereby, the minimal drift voltage for which an Argon escape peak is seen, $200 \text{ V/mm} = 2 \text{ kV/cm}$, is only exceeded for the 3 cm drift case. Therefore, a higher operational voltage would have to be applied to larger distances to avoid recombination.

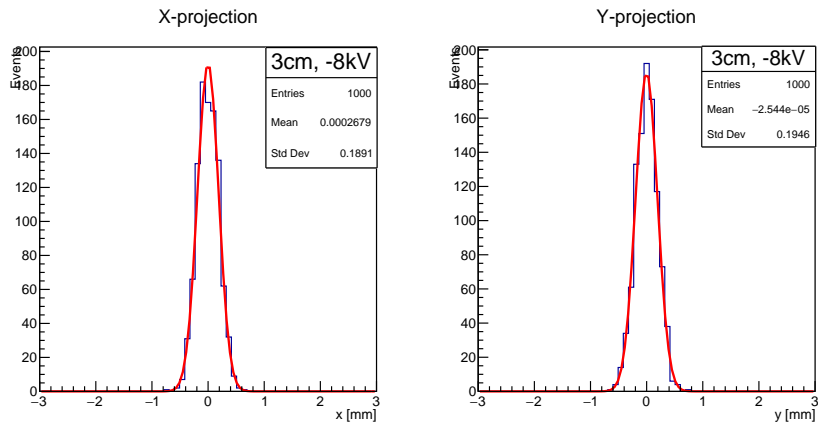
Since the electrons drift faster through the volume, the diffusion time for the spread in x and y direction is reduced and the cloud size becomes smaller for the same pressure. The information obtained from the simulations were used in order to design the new backgammon shaped readout plane shown above. This readout plane will be used in future work to experimentally investigate the cloud size.

Additional graphs of the results can be found in the appendix, section 8.1.

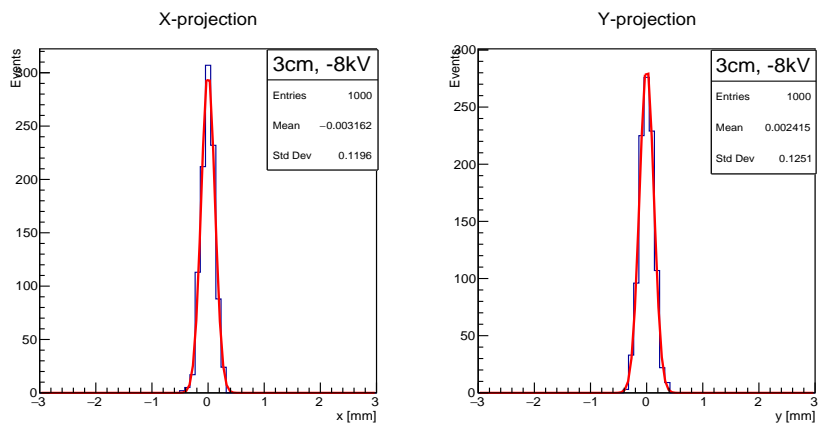
4 Simulation



(a)



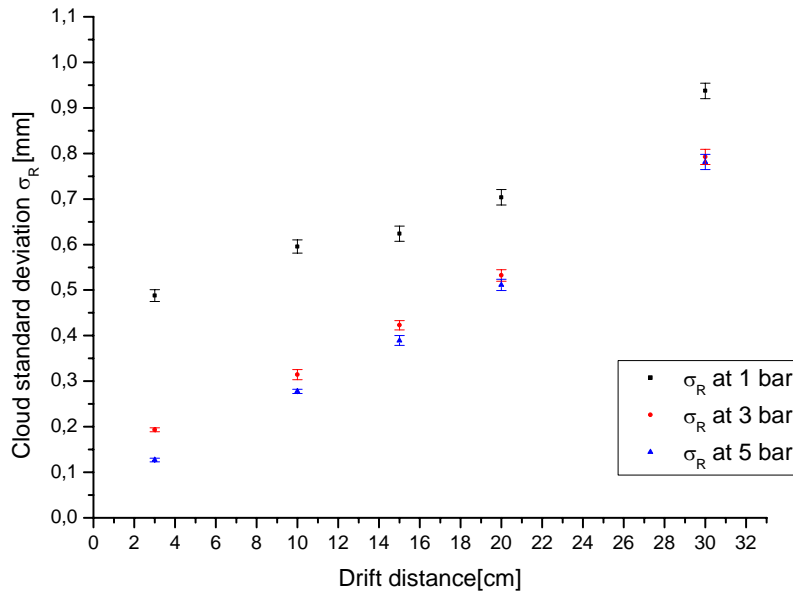
(b)



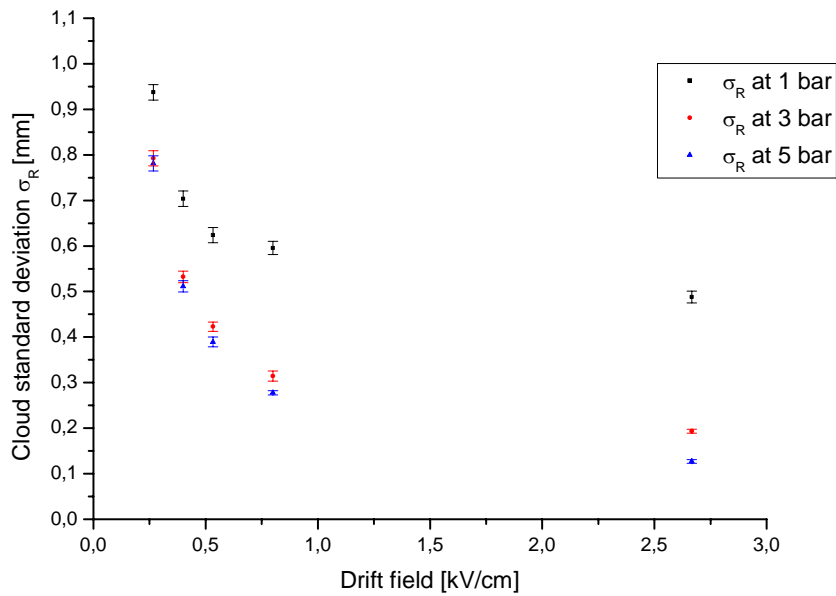
(c)

Figure 4.4: Simulation of the electron distribution for a drift length of 3 cm drift, 1000 electrons, and at pressures:(a) 1 bar, (b) 3 bar, (c) 5 bar. The total voltage is 8 kV.

4 Simulation



(a)



(b)

Figure 4.5: Panel(a): Electron cloud spread for varying pressures and varying drift distance, $U=8$ kV. Panel (b): Spread for different electric fields and varying pressures.

In both panels the spread is given by the standard deviation $\sigma_R = \sqrt{\frac{\sigma_x^2 + \sigma_y^2}{2}}$ from the Gaussian fit.

5 Data readout and Crosstalk

The overall goal for the development work is to extend the drift volume of the GEM detector so that a sufficient volume exists to inject the beam parallel to the plane defined by the GEM foil stack. The first test of this concept will use a source to introduce alpha particles directly into the volume. In order to test this setup, a dedicated gas tight Plexiglas box was manufactured and the test detector was placed inside of it.

The measurement of the rate and gain curves above used the summed signal from all strips on the readout board. However, in the final configuration it is necessary to read out each strip or pad individually to reconstruct the paths of the interacting particles. It is very beneficial if high-density electronics can be used for this purpose where amplifiers and ADCs are integrated on Application Specific Integrated Circuit (ASIC) chips. Such electronics have been developed e.g. for the ALICE TPC in a collaboration involving the ALICE group in the Particle Physics Division in Lund. In the second part of this thesis project this electronics was implemented. A data readout routine was written as part of the thesis work and in a first step the electronics was used to investigate potential cross talk that can influence the position resolution, e.g. have impact on the detected size of the electron cloud.

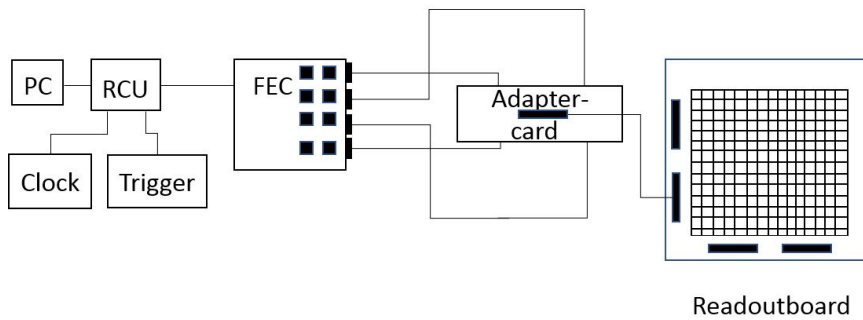


Figure 5.1: Diagram of the readout board electronics

A diagram of the complete setup used is shown in Figure 5.1. The readout strips are connected via a 130 channel Kapton cable fitted with Panasonic connectors using an adapter card, which seals the Plexiglas box, manufactured as part of this project. On the adapter card, four 40 channel Kapton cables are connected

5 Data readout and Crosstalk

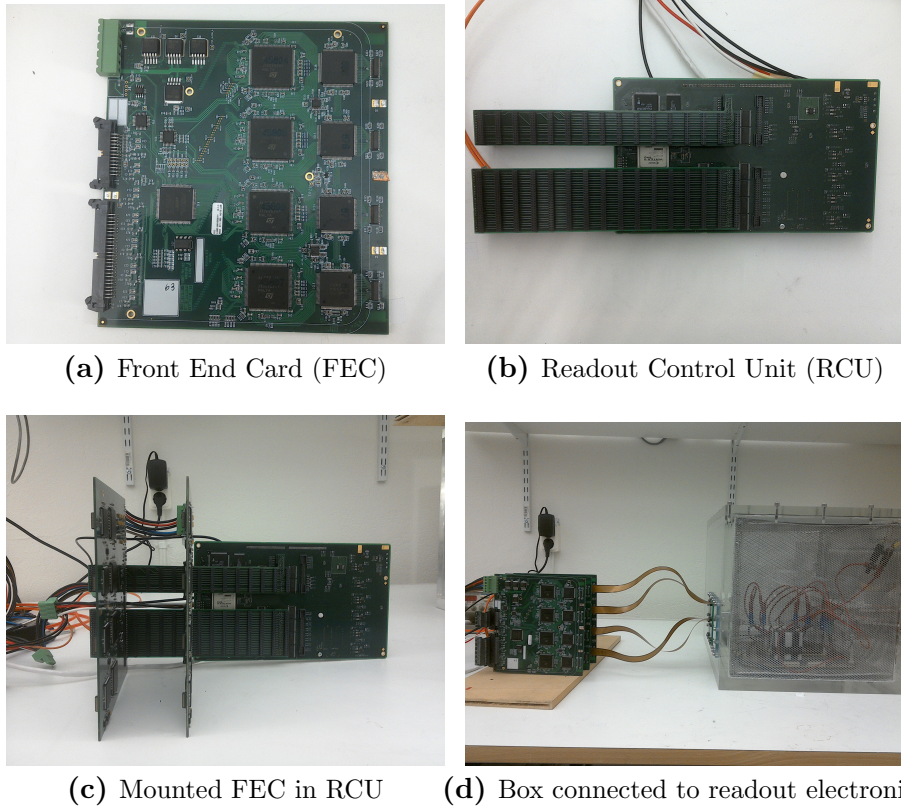


Figure 5.2: The readout components for the ALICE TPC ReadOut (ALTRO) Chips.

to the Front End Cards (FECs) for data readout using connectors from Japan Avionic Electronics (JAE). On each FEC, there are eight Programmable Charge Amplifiers (PCA16) and eight ALICE TPC Read Out (ALTRO) chips. The PCA16 converts the incoming charge to a digital signal using sampling Analogue to Digital Converters (sampling ADCs). This signal is processed by the ALTRO chip, which has 16 channels. The PCA16 settings can be changed to set the signal polarity, gain, and shaping times using different rise and decay times [17]. In total, one FEC has 128 channels, so that four channels of each JAE connector are grounded. The FEC is connected to a Readout Control Unit (RCU), which can control up to 32 FECs using a dedicated bus. The RCU is provided with a clock and a trigger, so that it can be programmed to run at different sampling frequencies. In this case, a sampling frequency of 20 MHz was chosen. Figure 5.2a - 5.2d show the components of this setup.

The data is sent to a Data ReadOut Receiver Card (DRORC) in the PC via an optical Detector Data Link (DDL). Data are stored in a raw binary file on the PC. Events can be monitored on a ROOT based histogram presenter, which is controlled via a Graphical User Interface (GUI). A picture of the GUI and an example of the registered amplitude vs time spectrum (trace) for the ALTRO

5 Data readout and Crosstalk

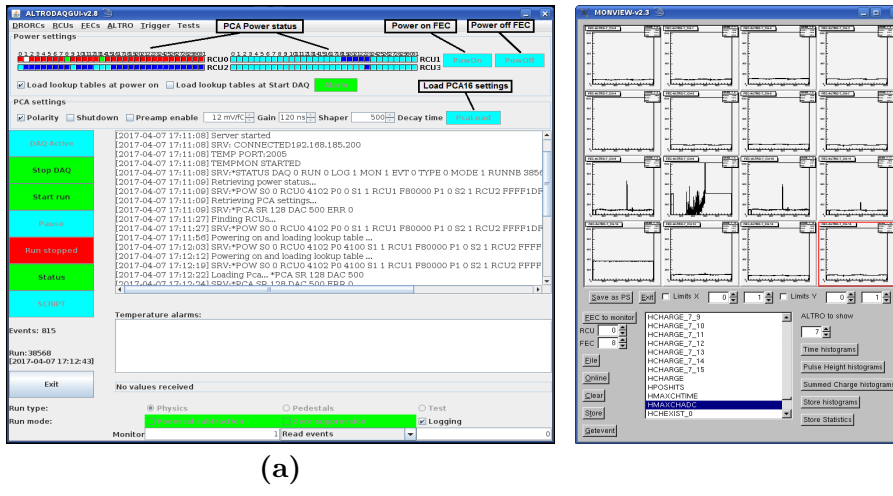


Figure 5.3: Panel (a): GUI, Panel (b): ALTRIO channel monitor, signal applied at FEC chn 121 = ALTRIO chn 7_9

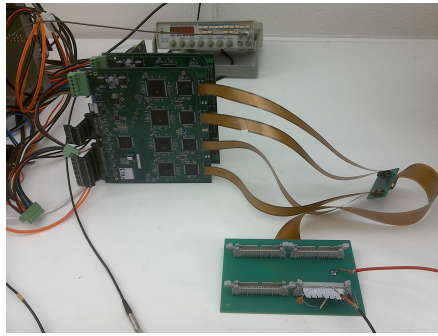
card (nr 7 in the setup) is given in Figure 5.3a.

When data is recorded with the help of the GUI, a raw data file is saved according to a given data format. In the analysis the file is decoded to give the channel where hits occurred, and the time and amplitude of the hits. A C++ program was written for this purpose as part of this project. In the following section, the raw data format is briefly explained according to Ref. [18].

The data format begins with a Start Of Run Record (SOR), which e.g. includes the run number and the PCA16 settings. The SOR is followed by an event header and a RCU header, which in turn is followed by the ALTRIO DATA. The data stream in a file ends with a corresponding End Of Run header (EOR). In case the maximal file size is reached, a Beginning Of File (BOF) and End Of File (EOF) header are saved in the raw data file, as well. All information is saved in binary data format.

As mentioned above, with the help of the definitions of the data stream in the file, data were decoded in a C++ program written in the ROOT framework. The program can present the incoming traces or histograms for the different channels where hits occurred. The principle of the program is to search for a beginning of run (given by 0×11111111) followed by the beginning of an event (0×22222222) until an end of a run (0×33333333) is reached. When the beginning of an event is found an ALTRIO DATA header is searched for in order to start decoding the information. The data are decoded and either presented as traces directly on screen, or the data is analysed with respect to signal amplitude. As part of this analysis thresholds can be set to avoid to trigger on noise when updating

5 Data readout and Crosstalk



(a)

Figure 5.4: Feeding of a signal into the ALLEGRO chip.

spectra. These software thresholds can also be used to analyse the amount of cross talk between channels. The code that was written is given in appendix 8.2 together with a more complete description of the data format. Due to the different connectors and cables, a mapping is needed to connect the respective FEC channel to a physical strip on the readout plane.

5 Data readout and Crosstalk

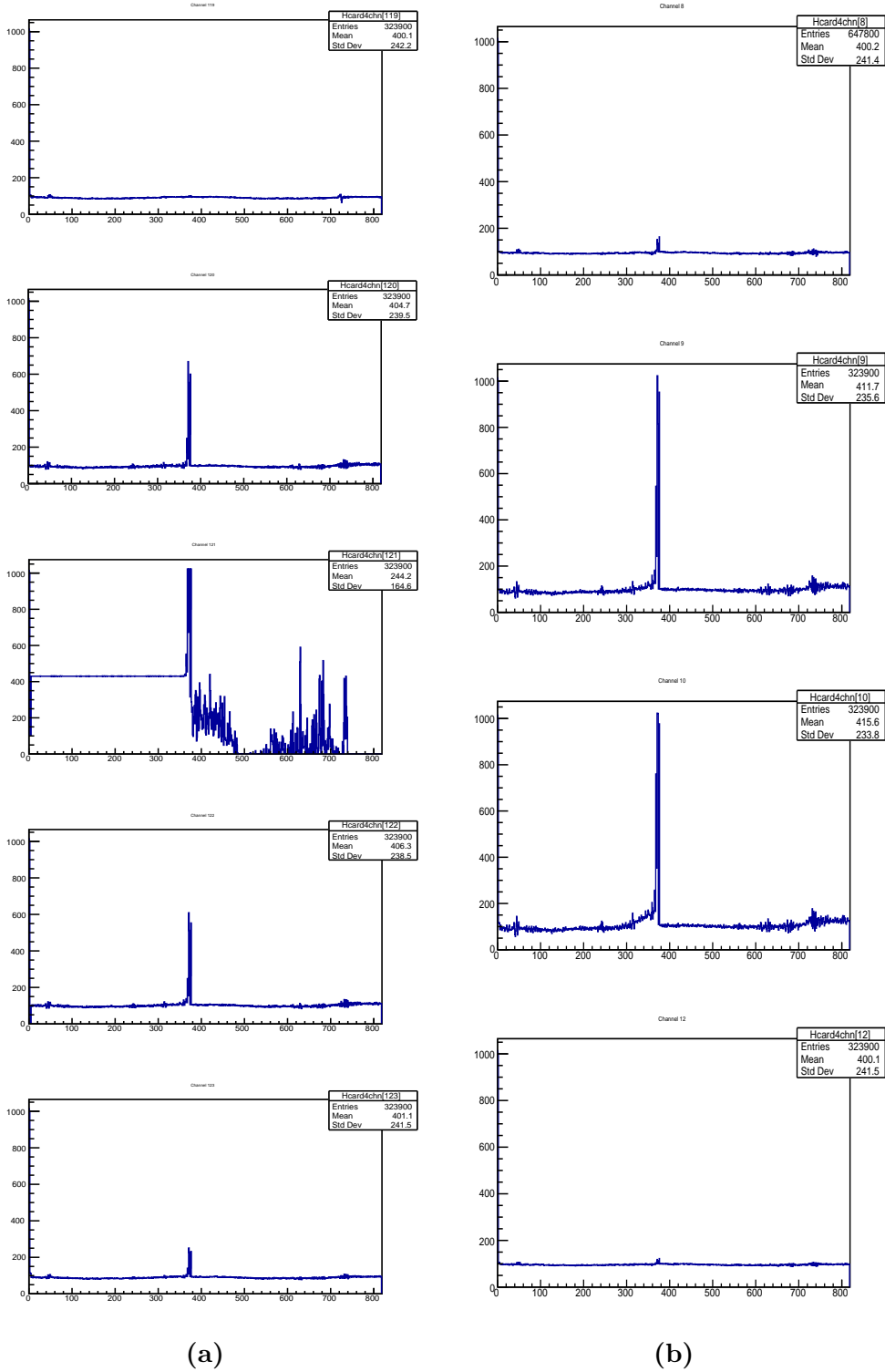


Figure 5.5: The measured traces, when a square pulse was applied to one input channel. In Panel (a), traces for channels 119 - 123, i.e. neighbouring channels on the ALTRO chip, for the case when a square pulse of 300 mV amplitude was applied over a 0.5 nF capacitor to channel 121. In Panel (b), the same 300 mV pulse is applied as in (a) showing the cross talk on the opposite sides of the 130 channel Kapton cable. The input overshoots the range of the input channel.

5 Data readout and Crosstalk

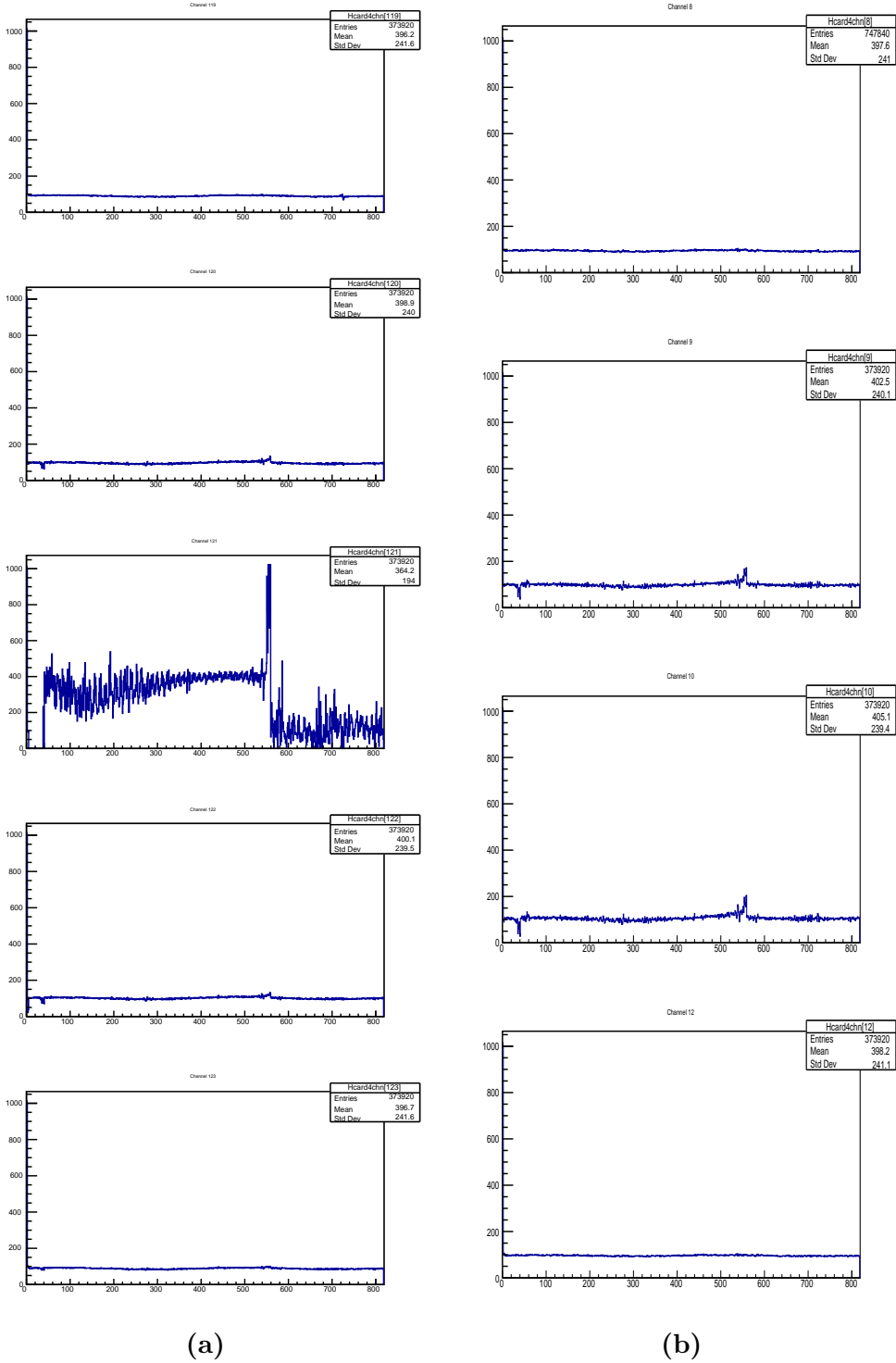
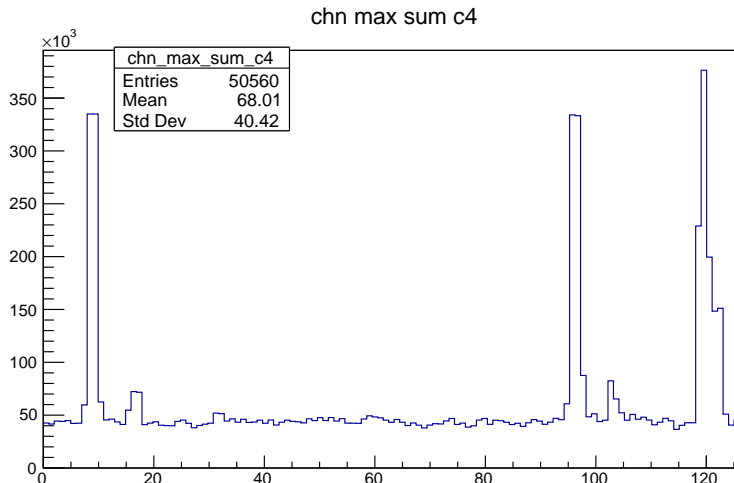


Figure 5.6: The measured traces, when a square pulse was applied to one input channel. In Panel (a), traces for channels 119 - 123, i.e. neighbouring channels on the ALTRO chip, for the case when a square pulse of 150 mV amplitude was applied over a 0.5 nF capacitor to channel 121. In Panel (b), the same 150 mV pulse is applied as in (a) showing the cross talk on the opposite sides of the 130 channel Kapton cable. One can note that the cross talk is significantly lower and close to the noise level. The amplitude of the input signal is here inside the range of the input channel.

5 Data readout and Crosstalk



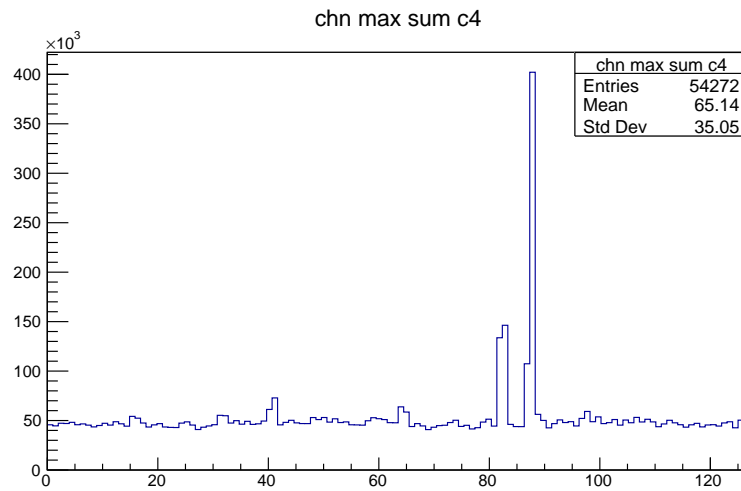
(a)

Figure 5.7: The histogram shows on the x-axis the channels that have triggered in the ALTRO chip when a 300 mV square pulse was fed in via the capacitor to channel 121, using a software threshold of 400.

To test cross talk on the cables and in the ALTRO card, that might influence the readout position resolution or hamper the identification of the correct strip, a square pulse signal was applied over a 0.5 nF capacitor to individual ALTRO channels. The cross talk was then investigated by varying the input voltage and adjusting the software threshold. For the test cases used clear cross talk could be seen when the input signal was above 200 mV over the 0.5 nF capacitor (see traces in Figures 5.5a, 5.5b, 5.6a, and 5.6b). Histograms showing which channels that triggered when the input amplitudes was above a given software threshold were created from the traces. These histograms were then compiled in order to see for which input amplitude and threshold it is possible to have a signal only on the channel where the input signal was applied (see Figures 5.7a and 5.8a).

The result from this investigation is summarized in Figure 5.9a. The conclusion of this test is that up to an input amplitude over the capacitor up to 200 mV it is possible to reduce cross talk with the help of a software threshold. This investigation gives important information when deciding about the gain of the GEM stack discussed in previous sections. A too high gain may give rise to an erroneous identification of the triggering strip. This investigation is also of interest when determining over how many channels cross talk would be acceptable for a certain strip width on the readout board.

5 Data readout and Crosstalk



(a)

Figure 5.8: The same histogram as in 5.7a when a 80 mV square pulse was fed in via the capacitor to channel 89, again using a software threshold of 400.

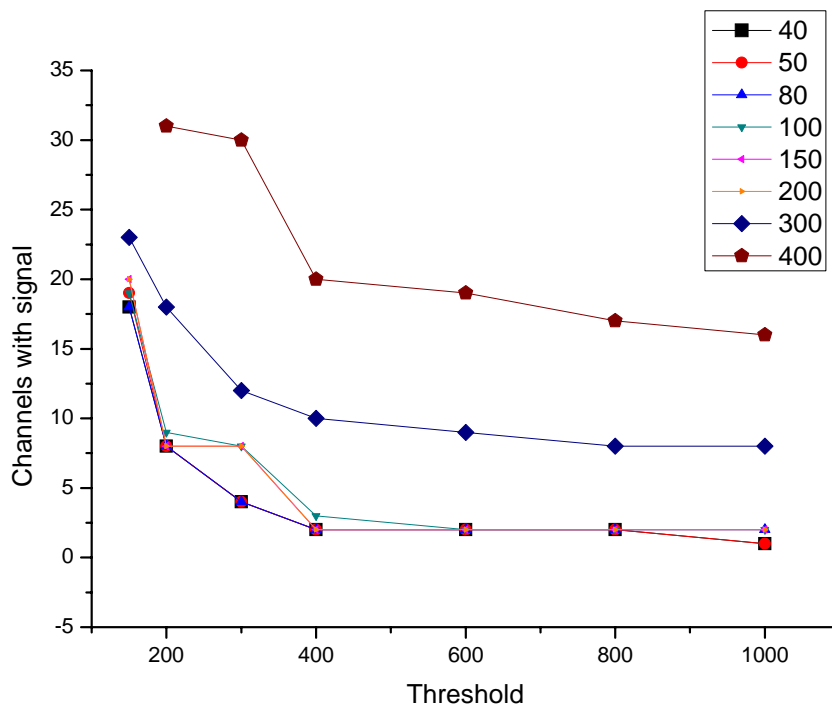


Figure 5.9: The number of channels with signals above a set software threshold for different amplitudes of the input pulse. The legend gives the input signal amplitude in mV.

6 Results and Conclusion

The existing GEM detector setup has been tested and extended. The mounting and commissioning of the GEM foils were performed in a clean fume hood instead of in a clean room. This approach turned out to be sufficient. The preparatory work with the foils is nevertheless time consuming. After being mounted in the GEM detector, the foils should be handled with care and the detector opened as seldom as possible to avoid dust to deposit on the foils and cause short circuits. Nevertheless, it was proven during this work that dust particles can be burnt off the foils without causing permanent damage. To avoid the risk of sparking on the voltage divider board, the GEM foils were also powered separately using different channels from a power supply.

Experience shows that in order to get a good signal, the grounding has to be controlled precisely, which took some time in the experimental part of the work. Due to the amount of time needed to test the foils, mount them in the detector and control the connections and grounding, it is time saving to use simulations instead of changing detector settings. Since the simulation reproduces the measurement results rather well, it makes it possible to save time that would otherwise be spent investigating small variations of the same detector.

For the setup with the voltage divider, rate curve and gain measurements were performed using a gas mixture of 82/18 Ar/CO₂ at a pressure of 1 bar and compared to previous results. Charge collection starts for this gas mixture at ≈ 3600 V. A plateau was reached for a rate of $f^* = 3644.1 \pm 28.4$ Hz. To calculate the gain of the detector, a current measurement was done at the readout plane. Using the amount of primary electrons created, for the test case, a gain of 80000 was deduced at total voltage of 4 kV. For the direct voltage supply setup, the plateau for the rate curve was reached for $f^* = 3711.1 \pm 23.6$ Hz. The gain at 4 kV was ~ 48000 .

For all measurements, a ⁵⁵Fe source was used, which produces a 5.9 keV X-ray when decaying, representing a minimum ionizing particle. Since the final aim of the detector is to track charged particles, a gas mixture with a higher amount of quencher is ideal, since the energy is absorbed by the quencher instead of creating more primaries. The risk of discharges is therefore reduced.

The simulation of the electron cloud distribution was split into two parts to reduce the computing time needed. For the width of the electron cloud after

6 Results and Conclusion

multiplication in the GEM detector, a value of ~ 1.2 mm was observed. The simulations of the transport through the drift region shows dependence on the applied pressure, electric field and the drift length. The higher the pressure, the longer the drift length and the lower the drift potential, the more often collisions with the gas atoms take place, which narrows the width of the cloud at the readout plane. The width of the electron cloud should, according to the simulations, typically be ~ 3 mm.

Tests of the readout electronics have been performed and a C++ program has been written to investigate cross talk. A square pulse with varying amplitude from a function generator was fed into the readout electronics via a capacitor. As expected, the cross talk decreased with decreasing amplitude and increasing software threshold. The information gained from this part of the work is of importance for determining the gain and therefore the number of GEM foils that should be used in the stack. It is also of importance to ensure that cross talk does not degrade position resolution or cause erroneous identification of hits on the readout plane.

7 Outlook

The next step in the development of the detector is to test it with another source. Instead of the ^{55}Fe source, which simulates the minimum ionizing particle, an alpha source should be used. Due to the large amount of energy deposited in the drift volume in that case, more primaries should be produced by the source. As a result, the number of amplification stages can probably be reduced, so that instead of three GEM foils only one could be sufficient to record a signal. Since mainly the GEM foils are prone to problems, possible risk of malfunction due to a damaged GEM foil would be reduced. Moreover, with a simplified setup the simulations performed with Garfield++ will require less computing time.

With the work described in this thesis, the development of the active target detector has progressed further. Nevertheless, there are several tests and simulations needed before the detector will be used in experiments.

8 Appendix

8.1 Drift and velocity simulation

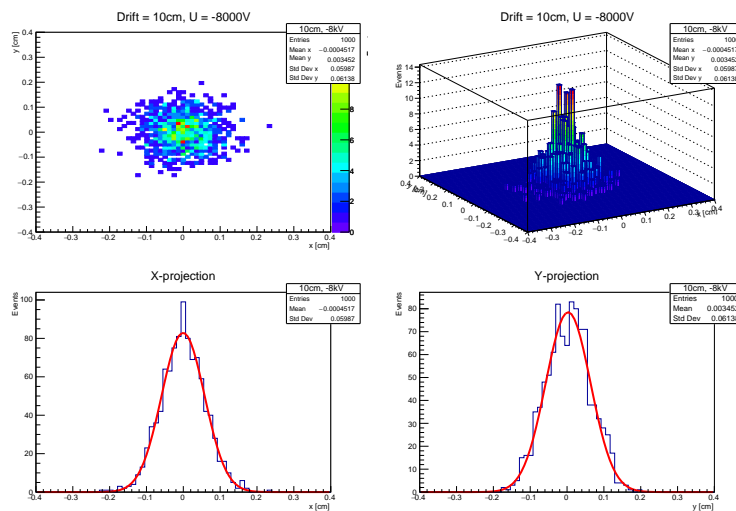


Figure 8.1: Drift 1bar 10cm

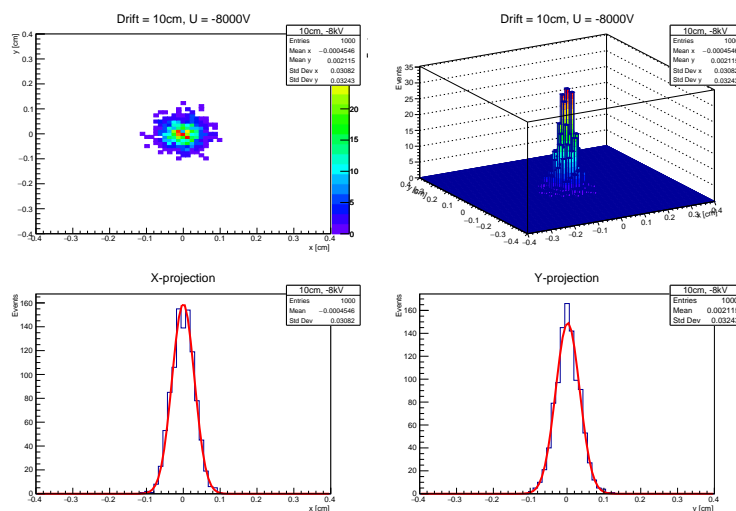


Figure 8.2: Drift 3bar 10cm

8 Appendix

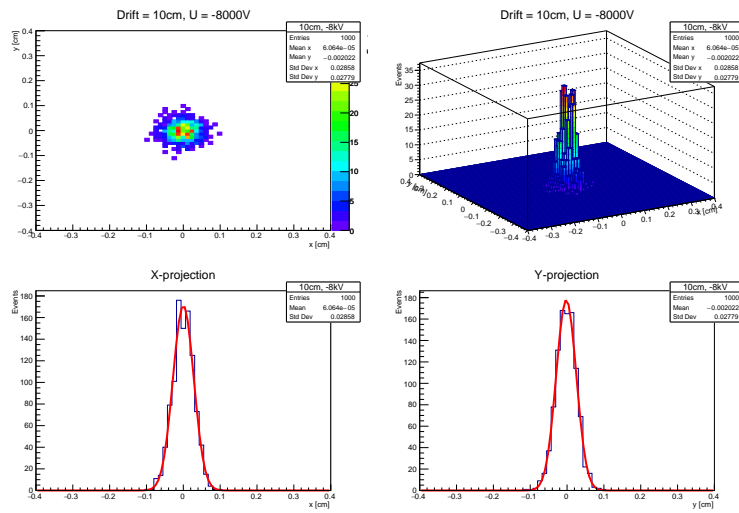


Figure 8.3: Drift 5bar 10cm

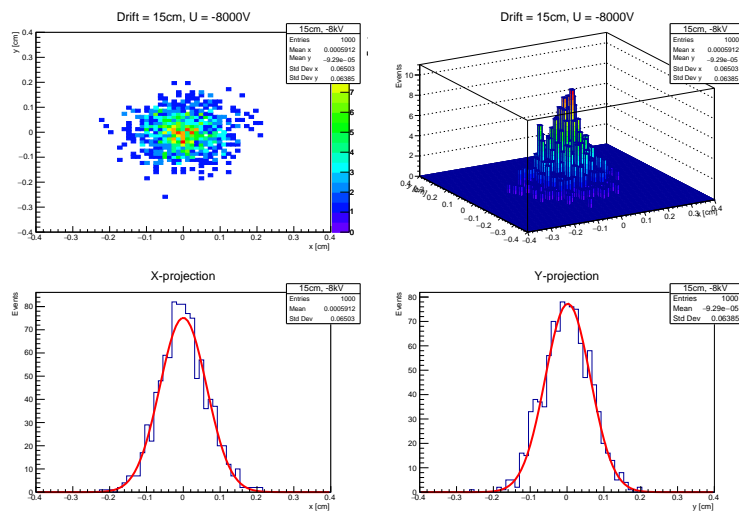


Figure 8.4: Drift 1bar 15cm

8 Appendix

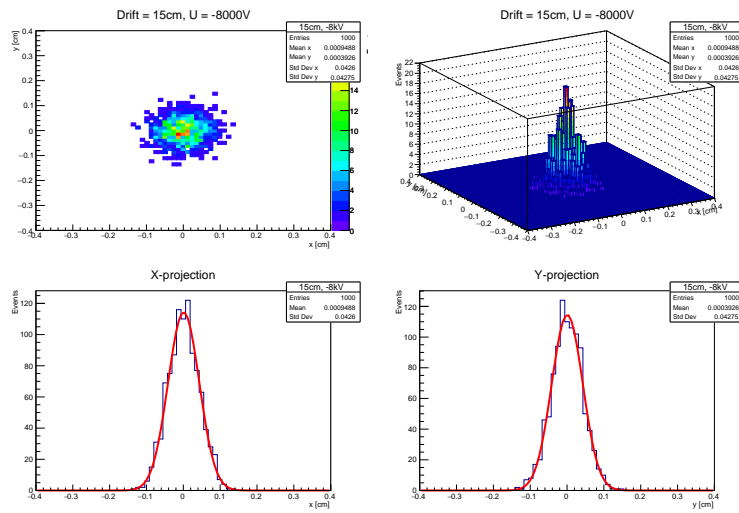


Figure 8.5: Drift 3bar 15cm

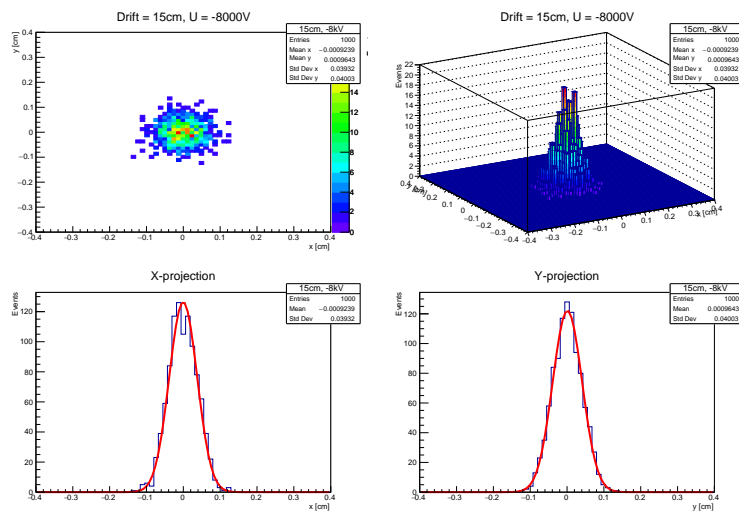


Figure 8.6: Drift 5bar 15cm

8 Appendix

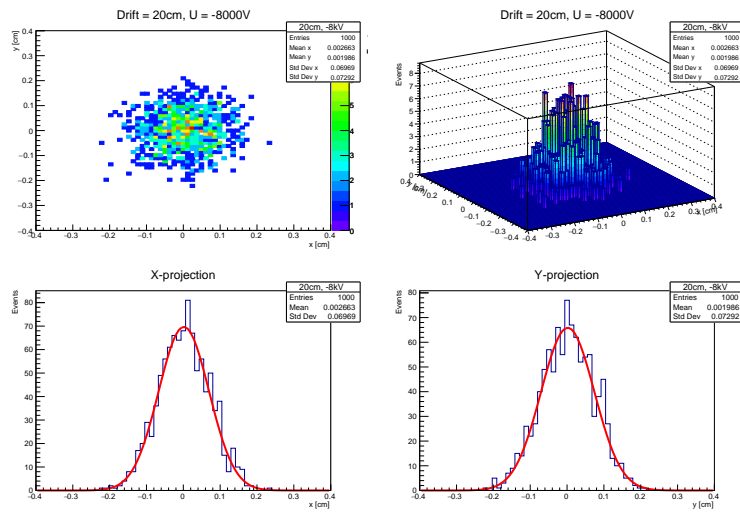


Figure 8.7: Drift 1bar 20cm

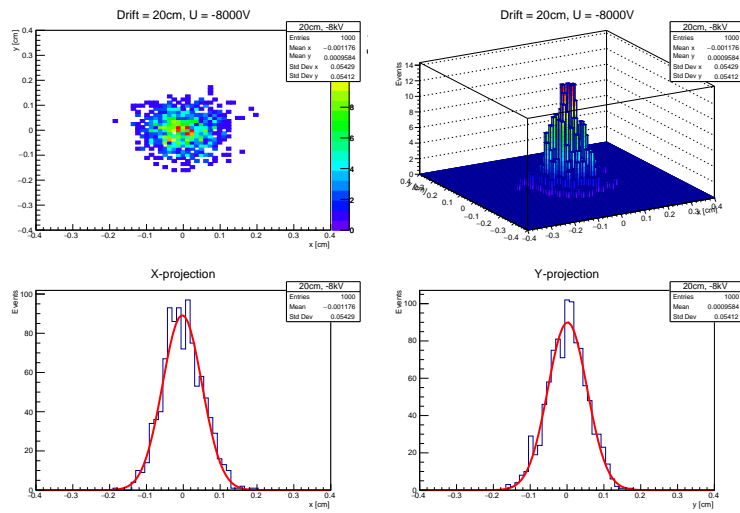


Figure 8.8: Drift 3bar 20cm

8 Appendix

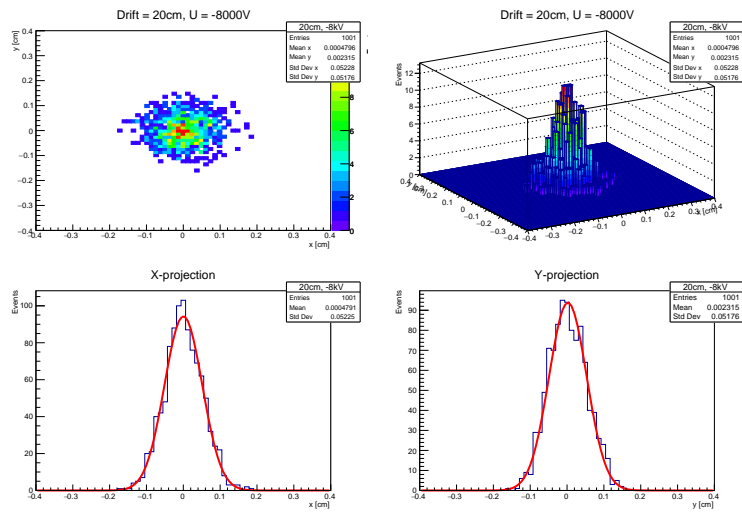


Figure 8.9: Drift 5bar 20cm

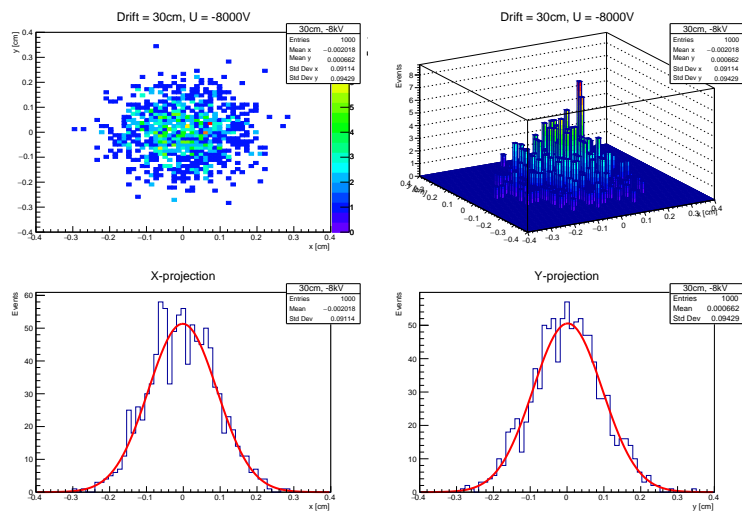


Figure 8.10: Drift 1bar 30cm

8 Appendix

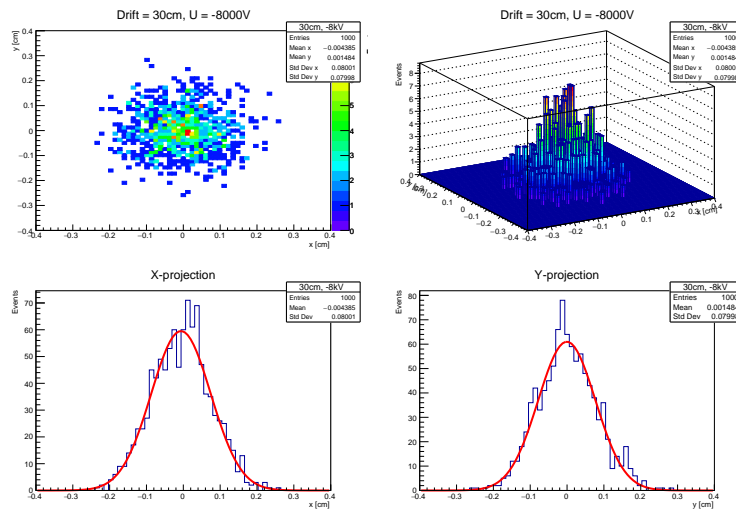


Figure 8.11: Drift 3bar 30cm

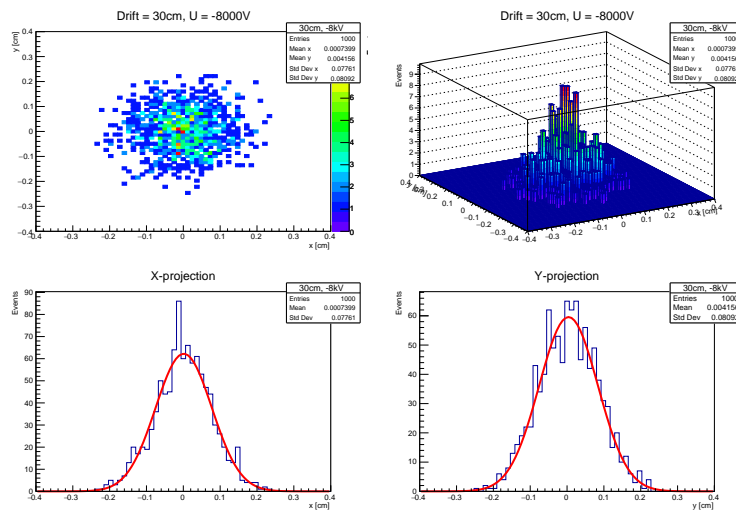


Figure 8.12: Drift 5bar 30cm

8.2 C-file

/* ALTRO FORMAT – 2017–03–21

OVERVIEW of RECORDS

–Start Of Run header (SOR)

–Event header

–Readout Controller Unit header (RCU)

–DATA

–End of Run header

+++++

8 Appendix

For cases where max file size is reached a

–Beginning of File header (BOF)

–End of File header (EOF)

is written as well

+++++

*****Beg SOR header

–Start of Run header

1. Length excluding word itself

XXXX|XXXX|

2. Header word exclusive length

XXXX|XXXX|

3. Block identifier SOR

1111|1111|

4. Data format and DAQ version

XXXX|XXXX|

 \ DAQ version (=47)

 \0 = reversed data format

 1 = 3 data words in reversed format

5. Run number

XXXX|XXXX|

6. Year – Month – Day

XXXX|XX|XX|

7. Hour – Minute – Second

XXXX|XX|XX|

8. Shiftreg setting and DAQ setting

XXXX|XXXX|

 | DAQ setting

Bit 0: preamp enable

 1–2: gain

 3–5: shaper

 6: shutdown

 7: polarity

9. Run settings

XXXX|XXXX|

Bit 0: zero supression

 1: pedastal subtraction

 2–3: samples above threshold (0–3)

 4–13: zero supression threshold (0–1023)

 14–16: number of postsamples (0–7)

 17–18: number of presamples (0–3)

 19–22: number of pretrigger samples (0–15)

 23–24: trigger source (1–data driven & parallell port, 2–DBOX, 3–data driven with DBOX)

10. EUDAQ run number

8 Appendix

```
XXXX|XXXX|
11. TSeconds
XXXX|XXXX|
number of seconds from clock_gettime
12. TNSeconds
XXXX|XXXX|
number of nano seconds from clock_gettime
*****End of SOR header
*****Beg of Raw event format
–Raw Event format
13. Total length
XXXX|XXXX|
14. Header length
XXXX|XXXX|
15. Block Identifier Event
XXXX|XXXX|
2222|2222|
16. Software Event number      SEN
XXXX|XXXX|
17. DBOX hardware trigger number
XXXX|XXXX|
18. DBOX timestamp
XXXX|XXXX|
19. TLUEVTNM TLU event number
XXXX|XXXX|
20. TSECONDS number of seconds as from function clock_gettime (added v4
    .6)
XXXX|XXXX|
21. TNSECONDS number of ns within second as from function clock_gettime (
    added v4.6)
XXXX|XXXX|
22. RCU block length (exclusive, added by software)
XXXX|XXXX|
23. RCU identifier (added by software)
XXXX|XXXX|
*****Beg of Readout Controller Unit
    header
–Readout Controller Unit header
24. Block length
XXXX|XXXX|
F// FFF|FFFF|
// 25. Format–type–id
// XXXX|XXXX|
// [11111111|XX|XXXXXXXXXX|00|XXXXXXXXXXXXXX]
```

8 Appendix

```

// Format      L1 type      Evt id 1
// 26. Evt id 2
// XXXX|XXXX|
// [00000000|XXXXXXXXXXXXXXXXXXXXXXXXXXXX]
//           Evt id 2
// 27. Block – subdetector
// XXXX|XXXX|
// [00000000|XXXXXXXXXXXXXXXXXXXXXXXXXXXX]
//   Block      subdetectors = 0
// 28. Status – bunch
// XXXX|XXXX|
// [0000|XXXXXXXXXXXXXXXXXXXX|XXXXXXXXXXXX]
//           status/error      bunch
// 29. Trigger classes low
// XXXX|XXXX
// 0000|0000|
// 30. ROI – trigger classes high
// XXXX|XXXX|
// [XXXX|000000000|000000000000000000]
// ROI           trigger classes high
// 31. ROI
// XXXX|XXXX|
// *****End of Readout Controller
//   Unit header
// *****Beg of DATA

// -DATA
// 32. ALTRO channel header
// XXXX|XXXX|
//   0100 0011 0011 0001
//   4   3   F   F   0   F   F   F
// [01X0|00XX|XXXX|XXXX|0000|XXXX|XXXX|XXXX]
//   E       \           channel number
//           nr 10 bit data words
// MAPS:

// Channel number: 00000FFF
// Nr of DW: 03FF0000 shift >> 16
// Type: 30000000

// 33. DATA words
// XXXX|XXXX|

```

8 Appendix

```
// [00|XXXXXXXXXX|XXXXXXXXXX|XXXXXXXXXX]
// ...
// *****End of DATA –
// *****Beg of Readout Controller
    Unit Trailer
// –Readout Controller Unit Trailer
// 33 + DATA. RCU TRAILER – 9 words
// Payload length
// XXXX|XXXX|
// Err reg 1
// XXXX|XXXX|
// Err reg 2
// XXXX|XXXX|
// Err reg 3
// XXXX|XXXX|
// Err reg 4
// XXXX|XXXX|
// FEC ro A
// XXXX|XXXX|
// FEC ro B
// XXXX|XXXX|
// RDO CFG1
// XXXX|XXXX|
// RDO CFG2
// XXXX|XXXX|
// RCU ID
// XXXX|XXXX|
// *****End of Readout Controller
    Unit Trailer

// *****Beg of EOR header
// –End of Run header
// Total length (exclusive)
// XXXX|XXXX|
// Header length (exclusive)
// XXXX|XXXX|
// Block identifier
// XXXX|XXXX|
// 3333|3333|
// Number of events
// XXXX|XXXX|
// Year–Month–Day
// XXXX|XX|XX|
// Hour–Minute–Second
```

8 Appendix

```
// XXXX|XXXX|
// TSeconds
// XXXX|XXXX|
// number of seconds from clock_gettime
// TNSeconds
// XXXX|XXXX|
// number of nano seconds from clock_gettime
// *****End of EOR header
```

```
// */
```

```
#include <ctype.h>
#include <math.h>
#include <TCanvas.h>
#include <TH1.h>
#include <TROOT.h>
#include <Riostream.h>
#include <stdio.h>
#include <string.h>
#include <TFile.h>
```

```
#define BEG_RUN 0x11111111
#define BEG_EVENT 0x22222222
#define END_RUN 0x33333333
#define DATA1_MAP 0x000003FF
#define DATA2_MAP 0x000FFC00
#define DATA3_MAP 0x3FF00000
#define WORDS_MAP 0x03FF0000
#define CARD_MAP 0x00000F00
#define CHN_MAP 0x000000FF
#define HEAD_MAP 0xC0000000
```

```
#define HEAD_TYPE 0x40000000
#define DATA_TYPE 0x00000000
```

```
//[00|1111111111|1111|1111|1111|1111|1111]
```

```
using namespace std;
```

```
void decode4() {
```

```
    Int_t i;
```

8 Appendix

```
UInt_t in_word;
Char_t in_buf [1];
ULong_t pos=0;
ULong_t tpos=0;
UInt_t nr_tb_words;
UInt_t nr_words;
UInt_t nr_word_2;
UInt_t pos_dw;
UInt_t dw_1;
UInt_t dw_2;
UInt_t dw_3;
UInt_t k_loop;
UInt_t chn_nr;
UInt_t card_nr;
UInt_t word_type;
UInt_t test;
Int_t index1,index2,index3;
Int_t max_val;
Int_t max_val_old;
Int_t th;

static int trace_array [16][128][820];

//create histos for our two cards

TH1I *h4[127]; //card 4
TH1I *h7[127]; //card 7

TH1I *mt3 = new TH1I("chn distribution", "chn distribution",128,0,127); //
distribution
TH1I *mt4 = new TH1I("chn max sum", "chn max sum",128,0,127); //max
sum

//one histo per channel
for (index2=0; index2<128;index2++){

    Char_t hname[15];
    Char_t htitle [15];

    sprintf( hname, "Hcard4chn[%d]", index2);
    sprintf( htitle, "Channel %d", index2);
    h4[index2] = new TH1I(hname,htitle,820,0,819);
```

8 Appendix

```
std::cout << "created:" << hname << "." << htitle << std::endl;

sprintf( hname, "Hcard7chn[%d]", index2);
sprintf( htitle, "Channel %d", index2);
h7[index2] = new TH1I(hname,htitle,820,0,819);

std::cout << "created:" << hname << "." << htitle << std::endl;
}

//4 canvases for plotting 64 channels each (Front End Card 4 and 7)

//TCanvas *c3 = new TCanvas("Card 7-1", "Card 7-1", 100,200,1200,900);
//TCanvas *c4 = new TCanvas("Card 7-2", "Card 7-2", 200,200,1200,900);
//TCanvas *c1 = new TCanvas("Card 4-1", "Card 4-1", 400,200,1200,900);
//TCanvas *c2 = new TCanvas("Card 4-2", "Card 4-2", 600,200,1200,900);

TCanvas *c7 = new TCanvas("Channel spectrum", "Channel spectrum",
    800,200,1200,900);
TCanvas *c8 = new TCanvas("Channel distribution", "Channel distribution
    ", 800,220,1200,900);

//c1->Divide(8,8);
//c2->Divide(8,8);
//c3->Divide(8,8);
//c4->Divide(8,8);

//select run
ifstream infile ("readout-34304_0.dat", ios::in | ios::binary);

if(! infile ) {
    cout << "Cannot open file.\n";
    //return 1;
}

TFile *mtr41 = new TFile("mt3_4_1.root", "update");

while(! infile .eof()) {

    infile .read(in_buf,4);
    in_word = *(unsigned int*) in_buf;
    pos = pos +4;
```

8 Appendix

```
//cout << "pos:" << pos << endl;

while (in_word==BEG_EVENT){
    //std::cout << "*****" << std::endl;
    //std::cout << "Beg of Event:" << in_word << "found at:" << pos
        << std::endl;
    //std::cout << "*****" << std::endl;

    //find first altro header at words after beginning of event
    for(int i=0; i<17; i++){
infile .read(in_buf,4);
in_word = *(unsigned int*) in_buf;
pos = pos+4;

        } //for i

    //this should be a header
    while ((in_word & HEAD_MAP) == HEAD_TYPE){
//std::cout << "*****" << std::endl;
//std::cout << "ALTRO header:" << hex << setw(8) << in_word << std
    ::endl;
//std::cout << "*****" << std::endl;

    chn_nr = (in_word & CHN_MAP);
    card_nr = (in_word & CARD_MAP)>>8;
    nr_tb_words = (in_word & WORDS_MAP)>>16;
    nr_words = nr_tb_words/3 + nr_tb_words%3;

    //std::cout << "Card nr:" << hex << setw(8) << card_nr << std::
        endl;
    //std::cout << "Channel nr:" << hex << setw(8) << chn_nr << std::
        endl;
    //std::cout << "Nr of ten bit words:" << hex << setw(8) <<
        nr_tb_words << std::endl;
    //std::cout << "Nr of words:" << hex << setw(8) << nr_words <<
        std::endl;

    //this should be a data word
    infile .read(in_buf,4);
    in_word = *(unsigned int*) in_buf;
    pos = pos+4;
    dw_1 = (in_word & DATA1_MAP);
    dw_2 = (in_word & DATA2_MAP)>>10;
```


8 Appendix

```
dw_3 = (in_word & DATA3_MAP)>>20;

//std::cout << "First data word:" << in_word << std::endl;
//std::cout << "dw_2:" << dw_1 << std::endl;
//std::cout << "dw_2:" << dw_2 << std::endl;
//std::cout << "dw_3:" << dw_3 << std::endl;

index1 = (Int_t) card_nr;
index2 = (Int_t) chn_nr;
index3 = (Int_t) 0; // first position

trace_array [index1][index2][index3]=dw_1;
trace_array [index1][index2][index3+1]=dw_2;
trace_array [index1][index2][index3+2]=dw_3;

//read out the number of words -1, check it is correct type
i=0;
while (((in_word & HEAD_MAP) == DATA_TYPE) & (i< int(nr_words
-1))) {

infile .read(in_buf,4);
in_word = *((unsigned int*) in_buf);
pos = pos+4;
i = i + 1;

dw_1 = (in_word & DATA1_MAP);
dw_2 = (in_word & DATA2_MAP)>>10;
dw_3 = (in_word & DATA3_MAP)>>20;

//std::cout << "Data word:" << in_word << std::endl;
//std::cout << "dw_2:" << dw_1 << std::endl;
//std::cout << "dw_2:" << dw_2 << std::endl;
//std::cout << "dw_3:" << dw_3 << std::endl;

index1 = (Int_t) card_nr;
index2 = (Int_t) chn_nr;
index3 = (Int_t) 3*(i+1);

trace_array [index1][index2][index3]=dw_1;
trace_array [index1][index2][index3+1]=dw_2;
trace_array [index1][index2][index3+2]=dw_3;
```

8 Appendix

```

} // while number of words

infile .read(in_buf,4);
in_word = *(unsigned int*) in_buf;
pos = pos+4;

//std::cout << "After channel readout:" << in_word << std::endl;

} // while next word is a header

//std::cout << "*****" << std::endl;
//std::cout << "Updating histos" << std::endl;
//std::cout << "*****" << std::endl;

//event has been read out, update histos and empty array
//we do it for our special case of FE card 4 and 7

//card 4
index1 = 4;
//loop over first 64 channels
for (index2=0; index2<64; index2++){

//loop over trace
for (index3=0; index3<820; index3++){

    h4[index2]->SetBinContent(index3,trace_array[4][index2][index3]);
}
h4[index2]->GetXaxis()->SetRange(10,819);
//      std::cout << "max histo:" << index2 << ":" << h4[index2
    ]->GetMaximum() << std::endl;

max_val = h4[index2]->GetMaximum();
max_val_old = mt4->GetBinContent(index2);
mt4->SetBinContent(index2,max_val+max_val_old);

th = 700;
if (max_val>th) {
mt3->Fill(index2);
//c8->cd();
    //mt3->Draw();
//gPad->Modified();
//gPad->Update();

```

8 Appendix

```

}

// update pads
//c1->cd(index2+1);
//c7->cd();
h4[index2]->GetXaxis()->SetRange(10,819);
//h4[index2]->Draw();
//gPad->Modified();
//gPad->Update();

} // loop over channel

//c7->cd();
//h4[index2]->Draw();
//gPad->Modified();
//gPad->Update();

//loop over second 64 channnels
for (index2=64; index2<128; index2++){

//loop over trace
for (index3=0; index3<820; index3++){

    h4[index2]->SetBinContent(index3,trace_array[4][index2][index3]);
    //cout << "index2:" << index2 << endl;
}
h4[index2]->GetXaxis()->SetRange(10,819);
//      std::cout << "max histo:" << index2 << ":" << h4[index2
    ]->GetMaximum() << std::endl;

max_val = h4[index2]->GetMaximum();
max_val_old = mt4->GetBinContent(index2);
mt4->SetBinContent(index2,max_val+max_val_old);

th = 400; //vary threshold between 200,400,1000
if ((h4[index2]->GetMaximum())>th) {
mt3->Fill(index2);
//c8->cd();
    //mt3->Draw();
//gPad->Modified();
//gPad->Update();
}
}

```

8 Appendix

```
// update pads
//c2->cd(index2+1-64);
//c7->cd();
//h4[index2]->Draw();
//gPad->Modified();
//gPad->Update();

} // loop over channel

//card 7
index1 = 7;
//loop over first 64 channels
for (index2=0; index2<64; index2++){

//loop over trace
for (index3=0; index3<820; index3++){

    h7[index2]->SetBinContent(index3,trace_array[7][index2][index3]);
}

// update pads
//c3->cd(index2+1);
//h7[index2]->Draw();
//gPad->Modified();
//gPad->Update();

} // loop over channel

//loop over second 64 channels
for (index2=64; index2<128; index2++){

//loop over trace
for (index3=0; index3<820; index3++){

    h7[index2]->SetBinContent(index3,trace_array[7][index2][index3]);
}

// update pads
//c4->cd(index2+1-64);
//h7[index2]->Draw();
//gPad->Modified();
//gPad->Update();
```

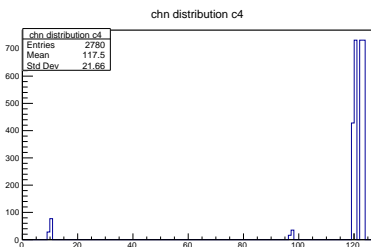
8 Appendix

```
    } // loop over channel

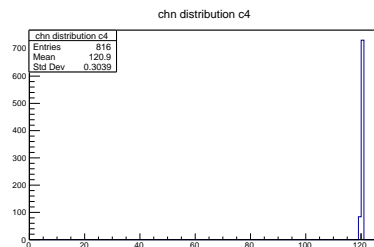
    } // while BEG_EVENT

} //while ! infile .eof()
infile .close();
mt3->Write();
mt4->Write();
mtr41->Close();

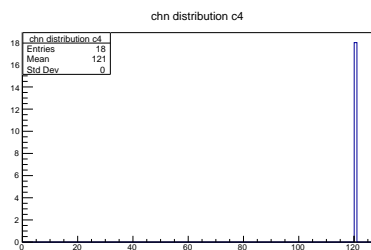
} //end of main
```



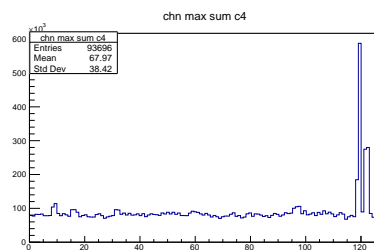
(a) 40mV th200



(b) 40mV th400



(c) 40mV th1000



(d) 40mV max chn entry

Figure 8.13: 40mV

8 Appendix

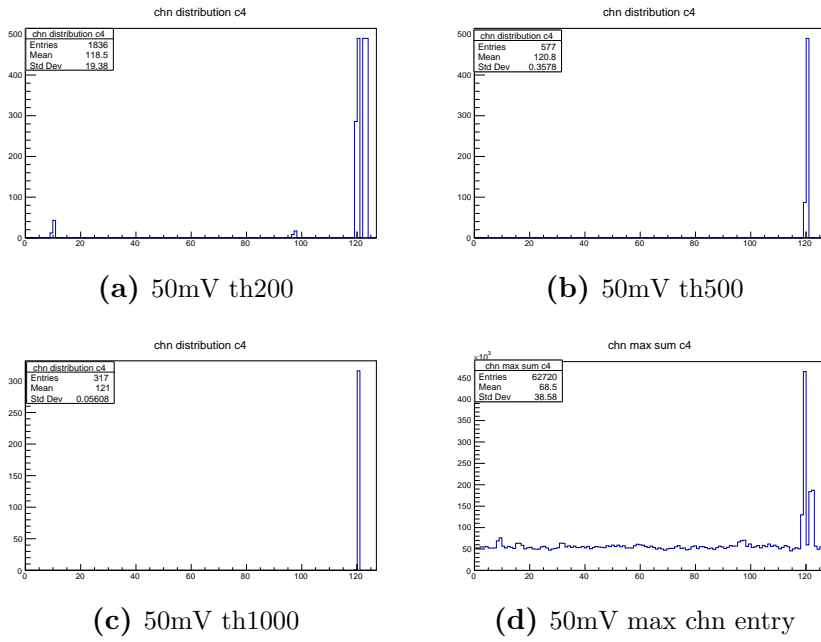


Figure 8.14: 50mV

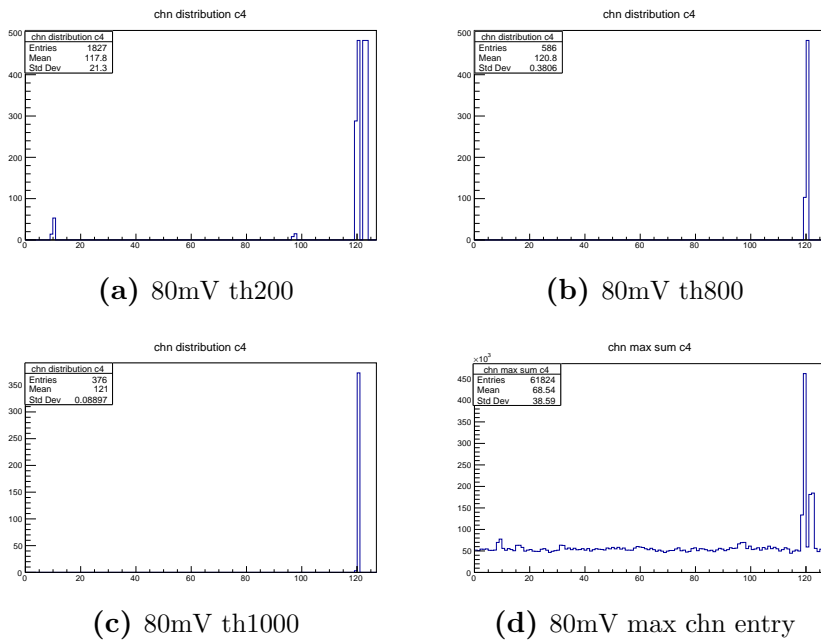


Figure 8.15: 80mV

8 Appendix

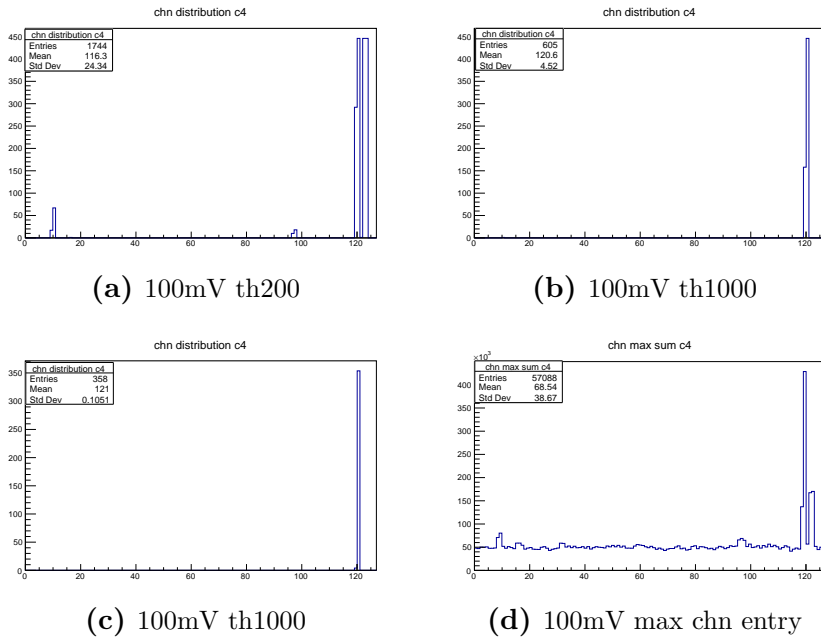


Figure 8.16: 100mV

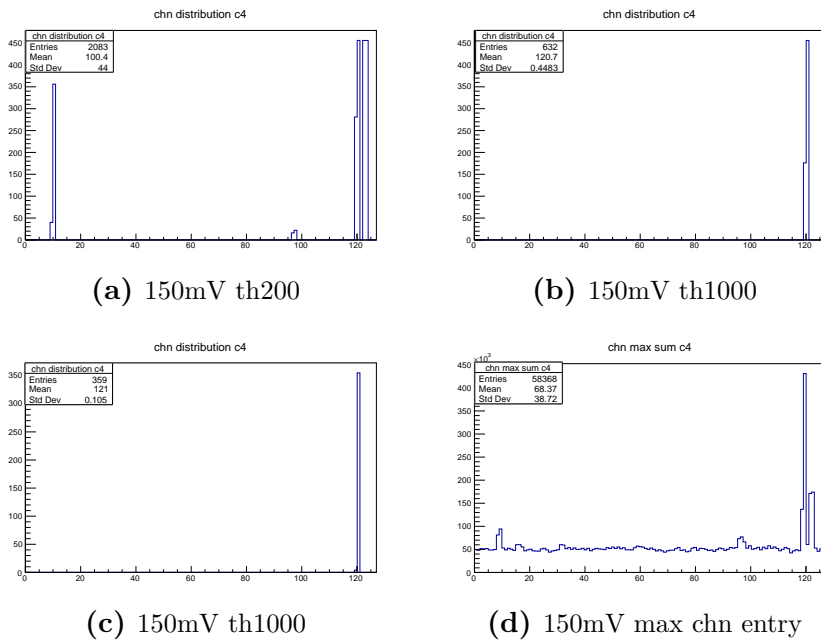


Figure 8.17: 150mV

8 Appendix

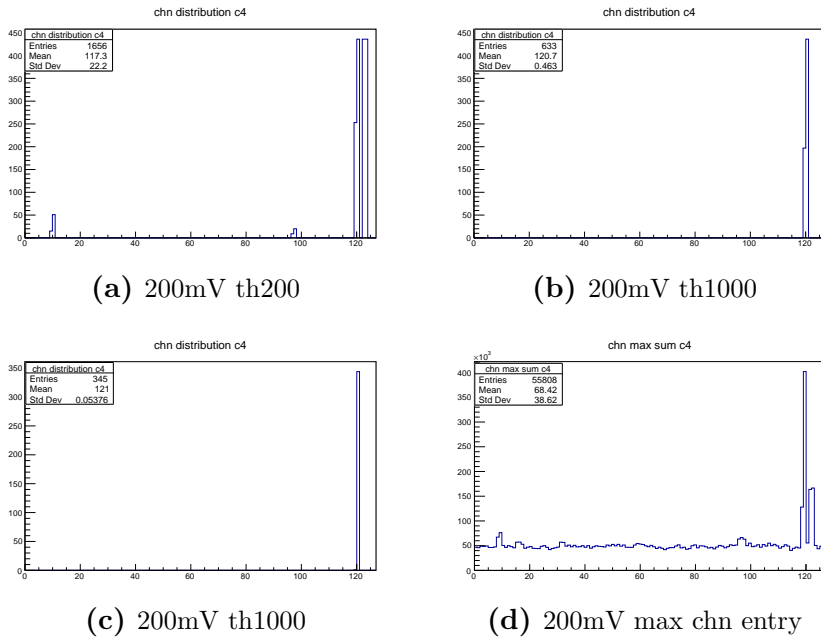


Figure 8.18: 200mV

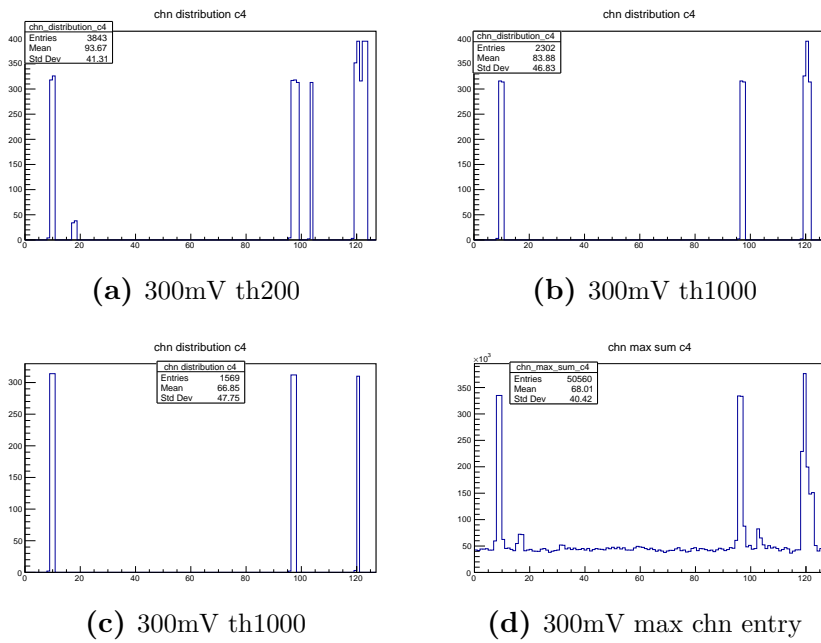
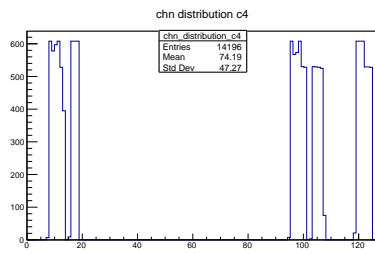
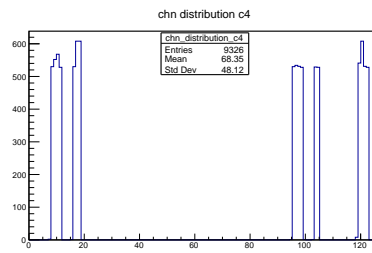


Figure 8.19: 300mV

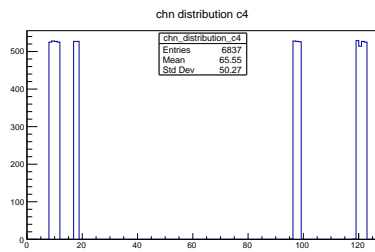
8 Appendix



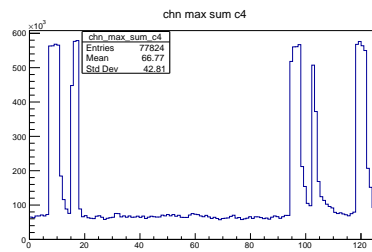
(a) 400mV th200



(b) 400mV th1000



(c) 400mV th1000



(d) 400mV max chn entry

Figure 8.20: 400mV

Acknowledgements

For this project, I got support from several persons, I would like to say thank you. I would like to especially thank my supervisor Joakim Cederkäll, who gave me the opportunity to come to Lund and supported and guided me. Tack så mycket!

Thanks to Pavel Golubev, for perform a big amount of small tasks (e.g. soldering), which saved a lot of time for me.

Concerning the work with the ALICE TPC Readout electronics, I would like to thank Ulf Mjörnmark, who took time to explain the setup and helped with starting the data acquisition.

Klaus Wendt I want to thank for his support of my thesis from abroad.

En stor tack goes to all the people at the nuclear physics department, who were always welcoming and created a wonderful working atmosphere.

Further more, I would like to thank my family and friends, who supported me from the background.

Bibliography

- [1] R.K. Wallace & S.E. Woosley: *Explosive Hydrogen Burning*, The Astrophysical Journal Supplement Series 45:389-420, 1981
- [2] J. Snäll: M.Sc thesis: *Test and simulations of GEM foils for use in an active target gaseous detector*, Lund University, 2016
- [3] S. Tavernier: *Experimental Techniques in Nuclear and Particle Physics*, Springer, 2010
- [4] F. Sauli: *Gaseous Radiation Detectors: Fundamentals and Applications*, Cambridge University Press, 2014
- [5] T. Tamagawa et al: *Development of thick-foil and fine-pitch GEMs with a laser etching technique*, Nuclear Instruments and Methods in Physics Research A, 608:390-396, 2009
- [6] Actar Collaboration, A. Chbihi et al: *An active target detector for study of extremely exotic nuclei*, Ganil, 2009.
- [7] F. Sauli: *GEM: A new concept for electron amplification in gas detectors*, Nuclear Instruments and Methods in Physics Research A, 386:531-534, 1997
- [8] S. Bachmann et al: *Discharge studies and prevention in the gas electron multiplier (GEM)*, Nuclear Instruments and Methods in Physics Research A, 479:294-308, 2002
- [9] J. Benlloch et al: *Further developments and beam tests of the gas electron multiplier (GEM)*, Nuclear Instruments and Methods in Physics Research A, 419:410—417, 1998
- [10] B. Yu: PhD thesis: *Gas proportional detectors with interpolating cathode pad readout for high track multiplicities*, University of Pittsburgh, 1991
- [11] Z. Gosser: M.Sc Thesis: *Using induced signals to sense position with a microchannel plate detector*, Indiana University, 2012
- [12] ROOT Data analysis software, Version 6.04.14. <https://root.cern.ch/>. Accessed: 10.10.2016
- [13] gmsh, Version 2.13.2. <http://gmsh.info/> Accessed: 10.10.2016
- [14] CSC-IT Center for Science LTD. Elmer, Version 8.3. <https://www.csc.fi/web/elmer/elmer>. Accessed: 09.11.2016

Bibliography

- [15] Garfield++, Version v1r0. <http://garfieldpp.web.cern.ch/garfieldpp/>. Accessed: 10.01.2017
- [16] Ö.Sahin et al: *Penning transfer in argon-based gas mixtures*, Journal of Instrumentation, P05002, 2010
- [17] HEP division Lund: *Instructions for testbeam 2016 (DAQ version 4.7)*, <http://www.hep.lu.se/eudet/daq/doc/instructions-201209.pdf> Accessed: 11.02.2017
- [18] HEP division Lund: *Raw data format*, <http://www.hep.lu.se/eudet/daq/doc/dataformat-v4.2-4.5.pdf> Accessed: 11.02.2017
- [19] F. Ames et al: *REX-ISOLDE Design and commissioning report*, CERN, 2005
- [20] M.A. Fraser et al: *Beam dynamics design studies of a superconducting radioactive ion beam postaccelerator*, Physical Review Special Topics - Accelerators and Beams 14.2, 2011
- [21] K. Markenroth, PhD thesis: *Exploring the Exotic - Experimental investigations far from stability*, Göteborg University, 2001
- [22] K. Markenroth et al: *Crossing the dripline to ^{11}N using elastic resonance scattering*, Physical Review C, VOLUME 62:034308, 2000
- [23] T. Mizogawa et al: *New readout technique for two-dimensional position-sensitive detectors*, Nuclear Instruments and Methods in Physics Research A, 312:547-552, 1992
- [24] A. Sharma: *Properties of some gas mixtures used in tracking detectors*, SLAC-J-ICFA-16-3, 1998
- [25] A. Sharma & F.Sauli: *First Townsend coefficient measured in argon based mixtures at high fields* Nuclear Instruments and Methods in Physics Research A, 334:420-424, 1993

List of Figures

1.1	Overview of the ISOLDE facility	2
1.2	Design of the detector under development	3
2.1	Normalized avalanche size probability	7
2.2	Avalanche formation and operation regions for gaseous detectors .	8
2.3	Working principle and photo of a GEM	9
2.4	Principle of a TPC	11
2.5	Used readout plane (256×256 strips)	13
2.6	MWBC Principle	14
3.1	Current test of a new GEM foil. The voltage is applied via the fan connectors.	16
3.2	Assembly of the GEM detector.	17
	(a) GEM foil with fans	17
	(b) Epoxy frame with gas inlets	17
	(c) Mounted GEM foils	17
	(d) Kapton window	17
	(e) Mounted GEM foils with frame	17
	(f) Mounted GEM foils - sideview with spacers	17
3.3	Circuit diagram of the voltage divider and the measurement setup.	19
3.4	First setup of the GEM detector	20
3.5	Rate curve for the 82/18 Ar/CO ₂ gas mixture. Charge collection starts at a total voltage of ca 3.7 kV and reaches a plateau at ca 3.9 kV when all events occurring in the sensitive volume give rise to a signal on the readout plane.	21
3.6	Current measurement for the 82/18 Ar/CO ₂ mixture.	23
3.7	Gain curve for the 82/18 Ar/CO ₂ gas mixture	24
3.8	Spectra for the different setups	25
3.9	Spectra for different voltages	26
3.10	Long term measurement	27
3.11	Rate curve measurement and gain curve estimation for the 82/18 Ar/CO ₂ gas mixture. Panel (a): Rate curve measurement for the direct voltage supply setup. Panel (b): Gain curve estimation. . .	27
4.1	gmsh geometry of a GEM foil	29

List of Figures

4.2	Elmer output for the GEM foil section. Panel (a): Mesh structure of electric field over GEM foil section. Panel (b): Calculated equipotential surfaces for the GEM foil section.	30
4.3	Avalanche simulation	33
4.4	Simulation of the electron distribution for a drift length of 3 cm drift, 1000 electrons, and at pressures:(a) 1 bar, (b) 3 bar, (c) 5 bar. The total voltage is 8 kV.	34
4.5	Electron cloud spread for varying pressures	35
5.1	Diagram of the readout board electronics	36
5.2	The readout components for the ALICE TPC ReadOut (ALTRO) Chips.	37
	(a) Front End Card	37
	(b) Readout Control Unit (RCU)	37
	(c) Mounted FEC in RCU	37
	(d) Box connected to readout electronics	37
5.3	Test of the readout electronics	38
5.4	Test of the readout electronics	39
5.5	Trace of a 300 mV square pulse applied on channel 121	40
5.6	Trace of a 150 mV square pulse applied on channel 121	41
5.7	Maximal channel entry	42
5.8	The same histogram as in 5.7a when a 80 mV square pulse was fed in via the capacitor to channel 89, again using a software threshold of 400.	43
5.9	Channels with signals for varying amplitude and thresholds	43
8.1	Drift 1bar 10cm	47
8.2	Drift 3bar 10cm	47
8.3	Drift 5bar 10cm	48
8.4	Drift 1bar 15cm	48
8.5	Drift 3bar 15cm	49
8.6	Drift 5bar 15cm	49
8.7	Drift 1bar 20cm	50
8.8	Drift 3bar 20cm	50
8.9	Drift 5bar 20cm	51
8.10	Drift 1bar 30cm	51
8.11	Drift 3bar 30cm	52
8.12	Drift 5bar 30cm	52
8.13	40mV	65
	(a) 40mV th200	65
	(b) 40mV th400	65
	(c) 40mV th1000	65
	(d) 40mV max chn entry	65
8.14	50mV	66

List of Figures

(a)	50mV th200	66
(b)	50mV th500	66
(c)	50mV th1000	66
(d)	50mV max chn entry	66
8.15	80mV	66
(a)	80mV th200	66
(b)	80mV th800	66
(c)	80mV th1000	66
(d)	80mV max chn entry	66
8.16	100mV	67
(a)	100mV th200	67
(b)	100mV th1000	67
(c)	100mV th1000	67
(d)	100mV max chn entry	67
8.17	150mV	67
(a)	150mV th200	67
(b)	150mV th1000	67
(c)	150mV th1000	67
(d)	150mV max chn entry	67
8.18	200mV	68
(a)	200mV th200	68
(b)	200mV th1000	68
(c)	200mV th1000	68
(d)	200mV max chn entry	68
8.19	300mV	68
(a)	300mV th200	68
(b)	300mV th1000	68
(c)	300mV th1000	68
(d)	300mV max chn entry	68
8.20	400mV	69
(a)	400mV th200	69
(b)	400mV th1000	69
(c)	400mV th1000	69
(d)	400mV max chn entry	69

List of Tables

3.1	Capacitances and leakage currents of the used GEM foils	16
3.2	The voltages applied across the different parts of the GEM detector using the voltage divider setup.	22
3.3	Direct voltage supply setup: Voltages across the different parts of the GEM detector	25